

1 Cellular thermometry considerations for probing 2 biochemical pathways

3 Manjunath C. Rajagopal¹ and Sanjiv Sinha^{1*}.

4 ¹*Department of Mechanical Science and Engineering,*

5 *University of Illinois at Urbana-Champaign, Urbana, IL 61801, USA.*

6 ABSTRACT

7 Extracellular thermometry has previously been used to probe cancer metabolism and
8 thermoregulation, with measured temperature changes of \sim 1-2 K in tissues, consistent with
9 theoretical predictions. In contrast, previous intracellular thermometry studies remain disputed due
10 to reports of >1 K intracellular temperature rises over 5 min or more that are inconsistent with
11 theory. Thus, the origins of such anomalous temperature rises remain unclear. An improved
12 quantitative understanding of intracellular thermometry is necessary to provide a clearer
13 perspective for future measurements. Here, we develop a generalizable framework for modeling
14 cellular heat diffusion over a range of subcellular-to-tissue length scales. Our model shows that
15 local intracellular temperature changes reach measurable limits (> 0.1 K) only when exogenously
16 stimulated. On the other hand, extracellular temperatures can be measurable (> 0.1 K) in tissues
17 even from endogenous biochemical pathways. Using these insights, we provide a comprehensive
18 approach to choosing an appropriate cellular thermometry technique by analyzing thermogenic
19 reactions of different heat rates and time constants across length scales ranging from sub-cellular
20 to tissues. Our work provides clarity on cellular heat diffusion modeling and on the required
21 thermometry approach for probing thermogenic biochemical pathways.

22 SIGNIFICANCE

23 Temperature is a fundamental thermodynamic property that can serve as a probe of biochemical
24 reactions. Recently, intracellular thermometry has gained attention since it could provide
25 unprecedented insights into subcellular metabolic pathways. In this work, we numerically show
26 that the intracellular temperature changes reach typical measurable limits of 0.1 K only if
27 externally stimulated. This is in stark contrast to certain previous experimental reports of > 1 K
28 change in subcellular organelles under endogenous conditions. Using a heat diffusion model that
29 accounts for thermal interfacial resistances in the cellular milieu, we provide guidelines on
30 choosing the right thermometry technique for a given type of biochemical reaction. In addition,
31 we show that the commonly used effective thermal conductivity parameter may fail to capture the
32 true temperature distribution, especially if the thermal interfacial resistances dominate the overall
33 heat diffusion.

34

35 **INTRODUCTION**

36 Biochemical reactions are often accompanied by enthalpy changes, resulting in local
37 temperature changes. This renders temperature a physiological parameter of interest that can
38 provide insights into biochemical pathways. For instance, extracellular thermometry has the
39 potential to detect cancer [1] and thyroid-related diseases [2], and for understanding multiple
40 metabolic pathways [3]–[6]. Such extracellular temperature changes originate in part from
41 intracellular metabolic reactions. Hence, there has been a growing interest in intracellular
42 thermometry [7]–[10] to probe sub-cellular metabolic pathways. However, studies using
43 intracellular thermometry have been widely debated due to disagreements with theoretical
44 predictions and potential measurement issues. For instance, previous studies [7], [11]–[17] report
45 localized intracellular temperature rise > 1 K for 5 min or more, which exceeds theoretically
46 predicted temperature changes [18]–[21] by several orders of magnitude. In some studies [7], [11]–
47 [14], [16], such intracellular temperature rises were never reported to go back to room
48 temperatures, arising questions on the theoretical plausibility [9], [18] of such results and their
49 measurement credibility. Potential measurement issues have been identified in certain
50 fluorescence-based thermometry techniques and are widely discussed in other recent reports [18],
51 [22]–[25]. On the other hand, the theoretical predictions of typical intracellular temperature
52 changes remain disputed [18]–[21], [26]. Baffou et al [18], [19] estimated that the typical
53 intracellular temperature changes don't exceed 10^{-5} K. Critics [9], [20], [21] have pointed out
54 incorrect assumptions of heat source, cell thermal conductivity, and length scale of heat sources.
55 Nonetheless, previous attempts [18]–[21], [26] to understand sub-cellular heat diffusion have been
56 unable to explain the experimentally observed intracellular temperature changes [7], [11]–[16]. In
57 contrast, at tissue length-scales, bioheat transport models [27], [28] with blood perfusion
58 assumptions were previously used to predict the tissue-scale temperature changes, which are in
59 good agreement with experimental results [4], [6], [27], [29]. Unlike tissue scale heat diffusion,
60 sub-cellular heat diffusion modeling is less explored, and previous approaches to these two length-
61 scales seem disconnected from each other. Therefore, there is a need for a unified approach to
62 modeling heat diffusion in biological cells spanning length scales ranging from sub-cellular to
63 tissues.

64 Here, we first reexamine the validity of the commonly used effective thermal conductivity
65 (k_{eff}) approximation at cellular length-scales. Typically, in a cellular milieu, the spatial variations
66 in thermal conductivity (k) are approximated as an effective thermal conductivity, k_{eff} , which is
67 often reported as the thermal conductivity itself. Resistance to heat diffusion not only stems from
68 the intrinsic material resistance, but also due to dissimilar material interfaces (Kapitza resistance,
69 R''_{TIR}) which often results in a discontinuous temperature jump across the interface [30]. The
70 cellular milieu is home to numerous dissimilar interfaces from biomolecular complexes such as
71 proteins, cytoskeleton components, organelles, etc. that are suspended in the cytosol. Such
72 biomolecular complexes with hydrophobic- or hydrophilic-water interfaces can result in R''_{TIR} of
73 $\sim 10^{-8}$ to 10^{-7} K.m²W⁻¹ [31]–[34] at a length-scale of ~ 50 nm. When interfaces dominate the overall
74 thermal resistance, an effective thermal conductivity may no longer model heat diffusion behavior
75 well. While the validity of k_{eff} has been questioned before [20], [26], this aspect has never been

76 explored in detail. Here, we show that the effective thermal conductivity can become length-
77 dependent if the interfacial resistances dominate, especially at cellular length-scales. We then
78 incorporate the interfacial resistances in our model to calculate the expected temperature changes
79 across sub-cellular to tissue length-scales. Our model helps to understand the typically expected
80 temperature changes and consequently the thermometry requirements for thermogenic reactions
81 of different timescales and heat rates. Overall, our work provides a cellular heat diffusion model
82 and the cellular thermometry requirements, which are vital for applications such as nanoparticle
83 heating of cryopreserved tissues [35], [36], thermal ablation of tumor cells [37]–[39],
84 thermometry-based bioenergetics studies [9], [40]–[42], etc.

85 This paper is organized as follows. The Methods section discusses the cellular heat
86 diffusion model, where we incorporate a cuboidal resistance network to capture the interfacial
87 resistances of biomolecular complexes. We validate our resistance network and the heat diffusion
88 model by comparing the results against the commonly used effective thermal conductivity
89 approximation. Using the validated heat diffusion model, we first discuss the typical endogenous
90 temperature changes at sub-cellular and tissue length-scales. We then highlight the implications of
91 the expected temperature changes in choosing a thermometry technique.

92

93 METHODS

94 Cellular heat diffusion model

95 Cells contain a variety of biomolecular complexes ranging from proteins and nucleic acids
96 to membranes and cytoskeleton to organelles such as lysosomes and mitochondria. Due to
97 collisions with other macromolecular compounds in the cytosol, molecular diffusion in the cytosol
98 has been estimated to be four times smaller than pure water [43]. The diffusion of heat, on the
99 other hand, has been relatively unexplored at sub-cellular length-scales [18]–[21], [26].

100 Heat transport in the cellular milieu can be assumed to be diffusive in nature, since the
101 molecular mean free path in liquids is much smaller than 1 nm. However, the subcellular region
102 contains biomolecular complexes that result in numerous dissimilar interfaces, where the diffusion
103 approximation is no longer valid [44]–[46]. One of the commonly used techniques to model the
104 thermal interfacial resistance at dissimilar surfaces is molecular dynamic (MD) simulations [47]–
105 [52]. For instance, studies using non-equilibrium MD simulations have captured the effects of
106 interface topography [53], curvature [52], size, bonding energy [49], etc. on the thermal interfacial
107 resistance. On the other hand, continuum models such as finite element methods (FEM)
108 approximate the temperature discontinuity across dissimilar interfaces using the interfacial
109 resistance as an input parameter [48], [54]. Typically, the thermal interfacial resistances are either
110 measured experimentally [33], [54] or calculated from MD simulations [48], [53]. MD based
111 simulations are usually limited to confined domains of few nm^2 – μm^2 and are also limited by the
112 computational capacity to be able to model an entire cell. To this end, in this work, we model the
113 heat transport in cells and tissues using finite element methods through COMSOL Multiphysics
114 software. While FEM cannot intrinsically estimate the thermal interfacial resistances, we instead

115 investigate heat transport for a range of possible interfacial resistances for the biomolecular
116 complexes. We discuss the range of values for the interfacial resistance shortly.

117 We model heat flow using the transient heat diffusion equation,

$$\nabla \cdot (k \nabla T) + \dot{Q}''' = \rho C_p \frac{\partial T}{\partial t} \quad (1)$$

118

119 where, T is the temperature, \dot{Q}''' is the volumetric heat generation rate, ρ is the density, C_p is the
120 specific heat, k is the thermal conductivity. Equation (1) is valid for diffusive heat transport across
121 a range of sub-cellular to tissue length-scales. However, at sub-cellular length-scales, the material
122 properties k , ρ , and C_p are a strong function of the spatial location due to the suspended
123 biomolecular complexes. Under steady-state conditions, the spatial variations of ρ and C_p can be
124 ignored. In a typical experimental measurement, the spatial variations in k and the effects of
125 additional interfacial resistances are approximated by an effective thermal conductivity, k_{eff} ,
126 which is often reported as the thermal conductivity itself. Previous work [18]–[21], [26] typically
127 used experimentally measured k_{eff} in a simplified version of Equation (1) to model the cellular
128 heat diffusion and for predicting the expected temperature changes. Instead, in this work, we
129 explicitly model the thermal interfacial resistance (R''_{TIR}) of biomolecular complexes by
130 introducing a temperature discontinuity at their surface, given by,

131

$$\Delta T = \frac{R''_{TIR} \dot{Q}}{A} \quad (2)$$

132

133 where, \dot{Q} is the rate of heat flow, and A is the surface area of the biomolecular complex.

134 Typical biomolecular complexes such as proteins are suspended in the cytosol with the
135 hydrophilic side chains exposed to saline, while the hydrophobic chains are curled inside. Such
136 hydrophilic-water interfaces are expected to have thermal interfacial resistance (R''_{TIR}) of $\sim 10^{-8}$
137 $\text{K} \cdot \text{m}^2 \text{W}^{-1}$ [31], [32]. For a hydrophobic-water interface, the interface resistance is typically higher
138 and is $\sim 2 \times 10^{-8} \text{ K} \cdot \text{m}^2 \text{W}^{-1}$ [33]. Highly hydrophobic materials such as carbon nanotubes have a
139 thermal interfacial resistance of $\sim 2 \times 10^{-7} \text{ K} \cdot \text{m}^2 \text{W}^{-1}$ with water [34]. Such interfacial resistances can
140 produce a considerable temperature change. For instance, if 1 nW of heat flows across a protein
141 chain of 50 nm width with $R''_{TIR} \sim 10^{-7} \text{ K} \cdot \text{m}^2 \text{W}^{-1}$, the temperature change can be as high as $\sim 20 \text{ mK}$
142 across a length of 100 nm. Further, when the interfacial resistances dominate the overall resistance
143 to heat diffusion, the effective thermal conductivity (k_{eff}) would be less than that of proteins
144 ($k_p \sim 0.1\text{--}0.2 \text{ W m}^{-1} \text{ K}^{-1}$). This can happen at sub-cellular length-scales and has recently been
145 observed in an intracellular effective thermal conductivity measurement [55], which reported a
146 $k_{eff} \sim 0.07\text{--}0.13 \text{ W m}^{-1} \text{ K}^{-1}$. To accurately capture the heat diffusion at sub-cellular length-scales,
147 Equation (2) must be used as a boundary condition at the surfaces of biomolecular complexes
148 while solving Equation (1). Moreover, the topology of the biomolecular complexes must be

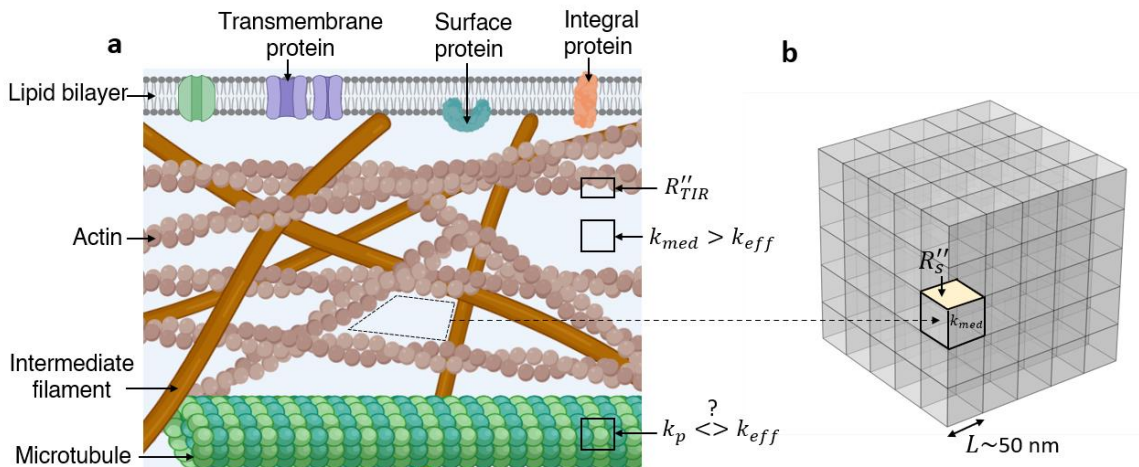
149 established to be able to model the interfacial resistances. Therefore, in the following section, we
 150 introduce a generalized cubical topology for the biomolecular complexes.

151 **A generalized resistance network**

152 Figure 1a shows a partial picture of the cellular components across a $\sim 0.1 \mu\text{m}^2$ area near
 153 the cell wall [56]. The cytoskeleton components such as actin, intermediate filaments, and
 154 microtubules are roughly 6 nm, 10 nm, 25 nm in diameter [57]. A steady-state heat diffusion across
 155 this subcellular space is subjected to a thermal resistance from the medium (t/k_{med}), the intrinsic
 156 resistance of proteins in the filaments (t/k_p) and the interfacial resistances of the filaments (R''_{TIR}),
 157 where t is the corresponding thickness. The thermal resistance network in the cellular environment
 158 can be visualized as numerous pockets of polyhedrons (filled with water) surrounded by protein
 159 chains. This can be approximated as cuboidal pockets of medium surrounded by surfaces of protein
 160 with a lumped resistance R''_S , as shown schematically in Figure 1b. The validity and impact of this
 161 approximation are discussed later, but we first explain the physical meaning of this lumped
 162 resistance R''_S . The resistance R''_S can be assumed to be a lumped representation of all the
 163 intracellular components and their interfacial resistances. A mathematical representation of R''_S is:
 164

$$R''_S \approx A \sum_i \frac{t_i}{k_{p_i} A_i} + \frac{R''_{TIR_i}}{A_i} - \frac{t_i}{k_{med} A_i} \quad (3)$$

165
 166



167
 168 Figure 1 a) Schematic of typical cytoskeleton components in a roughly $0.1 \mu\text{m}^2$ area near the cell wall.
 169 k_{eff} is the effective thermal conductivity of all the components shown here. If $k_p > k_{eff}$, the thermal
 170 interfacial resistance (R''_{TIR}) dominate the k_{eff} . b) A simplified representation of the thermal resistance
 171 network. The medium is assumed to have a thermal conductivity of k_{med} , surrounded by surfaces on all
 172 sides with a resistance of R''_S ($\text{K} \cdot \text{m}^2 \text{W}^{-1}$).

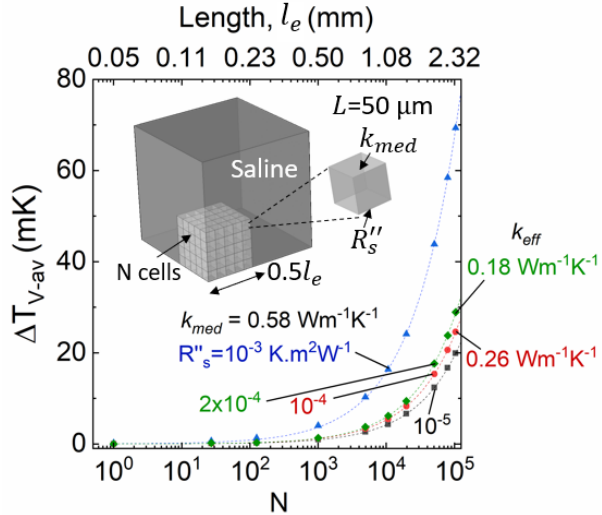
173
 174
 175 where, t_i is the thickness of a lipid/protein/organelle i with a thermal conductivity k_{p_i} ,
 176 effective surface area A_i , with an interfacial resistance R''_{TIR_i} , and A is the surface area of the
 177 individual unit ($\sim L^2$) along which R''_S is borne (Figure 1b). The last term in Eqn. (3) accounts for

178 the reduction in the medium's resistance due to displacement of the medium by the material i . Any
179 advection thermal resistance can also be a part of Eqn. (3). We henceforth call this resistance R''_s
180 as the equivalent thermal resistance at a length-scale L , since from Eqn. (3) we can see that R''_s is
181 a strong function of the length-scale $\sim At_i/A_i$. At a length-scale of $L \sim 50$ nm, R''_s is representative
182 of the resistances from protein chains, whereas, at a length-scale $L \sim 50$ μm , R''_s represents all the
183 proteins in the cell as an equivalent lumped resistance at the cell-wall. Thus, R''_s can be higher at
184 50 μm than at 50 nm. We now discuss the implications of a cuboidal resistance network
185 approximation. Unless stated otherwise, we assume in this work that the pockets are filled with a
186 medium, whose $k_{med} = 0.58 \text{ Wm}^{-1}\text{K}^{-1}$, corresponding to the thermal conductivity of water. The
187 real picture could be better represented by a k_{med} that is $< 0.58 \text{ Wm}^{-1}\text{K}^{-1}$, due to the dispersed
188 proteins and ions, and R''_s could be $\sum_i R_{TIR_i}$ instead of Eqn. (3). However, since an accurate spatial
189 distribution of k_{med} and R''_{TIR} is not available for a heterogeneous cellular environment, we assume
190 that all the additional resistances are lumped along the surface as R''_s (Eqn. (3)). Further, we assume
191 a rectilinear topology (cuboid) for the unit cell of the resistance network as shown in Figure 1b.
192 The real topology could be complex (with entangled resistance network and high interfacial
193 resistances) or simpler (with a homogenous dispersion of proteins and low interfacial resistance).
194 Our cuboidal resistance network may not be a unique representation, but we show in this work that
195 it serves well as a general example to understand the cellular heat diffusion picture.
196

197 RESULTS

198 Revisiting the effective thermal conductivity approximation

199 We revisit the effective thermal conductivity approximation and use it to validate our
200 cuboidal resistance network model. An effective thermal conductivity, k_{eff} , approximates the
201 local thermal resistances such that under a known amount of steady heat (Q), the temperature
202 change (ΔT) can be predicted using a single thermal property, k_{eff} . The effective thermal
203 conductivity is a function of the type of heat input (line, surface, or volumetric) [58], and the
204 location of the temperature measurement. Typically, the measured temperatures can be volume
205 averaged (T_{v-av}), surface average (T_{s-av}), volume maximum (T_{v-m}), or surface maximum
206 (T_{s-m}). For bio-heat transport studies, especially for thermometry-based bioenergetics studies, a
207 useful and an often-measured parameter is the average temperature in a volume (T_{v-av}). The T_{v-av}
208 is representative of an average temperature measured using fluorescent dyes, or dispersed
209 nanoparticles. If the heat input is known (say, endogenous heat source, or laser), the average
210 temperature change can be used to estimate the local effective thermal conductivity, k_{eff} [55],
211 [59]. Thus, in this study, we assume k_{eff} as the effective (or measured) thermal conductivity
212 calculated using the volume averaged temperature (T_{v-av}) for a known volumetric heat source.
213 We later discuss how the location of temperature measurement and the type of heat source affect
214 the effective thermal conductivity k_{eff} .



215

216 Figure 2. Volume averaged temperature change (ΔT_{v-av}) of the stack of cells is plotted against the
 217 number of cells, N , in the stack. The total edge length of the stack of cells is given by l_e , which is
 218 $\sim (NL)^{0.33}$, where L is the length of each cell surrounded by R''_s . The ΔT_{v-av} are shown for 4
 219 combinations of k_{med} and R''_s , as shown inside the graph. For lengths, $l_e > 1$ mm, the plotted ΔT_{v-av} also
 220 correspond to a stack of cells with an effective thermal conductivity, k_{eff} , as noted outside the graph
 221 using the corresponding colors. Each cell is assumed to release heat of 2.5 nW. Only 1/8th of the domain
 222 is shown in the schematic for clarity.

223 Using the above-mentioned definition of effective thermal conductivity, k_{eff} , we now
 224 discuss how the cuboidal resistance network's k_{eff} prediction compare against those that were
 225 previously measured experimentally. Consider a stack of N cuboidal cells (Figure 2), representing
 226 a multi-cellular tissue. Each cell has an edge length, $L=50$ μ m, roughly corresponding to an adipose
 227 cell size [60]. The cells are assumed to be filled with a medium of thermal conductivity k_{med} ,
 228 surrounded by an equivalent surface resistance, R''_s . The stack of cells is surrounded by saline. A
 229 constant outer surface temperature (20°C) is assumed at the saline far from the tissue. At large
 230 length scales, $l_e \gg R''_s k_{med}$, where $N \rightarrow \infty$, the effective (or measured) thermal conductivity of
 231 the tissue can be analytically approximated as,

$$k_{eff} = \frac{L}{R''_s + \frac{L}{k_{med}}} \quad (4)$$

232 We computationally confirm the effective thermal conductivity approximation (Eqn. (4))
 233 using Figure 2. We use finite element simulations that were validated for interfacial resistance
 234 modeling in our previous work [40], [54], [61] and for modeling transients in the supplementary
 235 material. A nominal volumetric heat of 2.5 nW is assumed to be released per cell, which
 236 corresponds to a typical cell metabolism rate [41], [62]. We plot in Figure 2 the volume-averaged
 237 temperature change (ΔT_{v-av}) in the cell stack against the number of cells, N , in the stack. ΔT_{v-av}
 238 is plotted for different equivalent resistances, R''_s from 10^{-3} to 10^{-5} $\text{K.m}^2\text{W}^{-1}$. We also plot the
 239 corresponding temperature changes without an equivalent resistance R''_s , but with an effective

240 thermal conductivity k_{eff} (0.18 and 0.26 $\text{Wm}^{-1}\text{K}^{-1}$), for $l_e > 1 \text{ mm}$, as marked outside the graph in
241 Figure 2. We specifically choose a k_{eff} of 0.18 $\text{Wm}^{-1}\text{K}^{-1}$ and 0.26 $\text{Wm}^{-1}\text{K}^{-1}$ since previous studies
242 report the effective thermal conductivity for adipose tissues to be in the range 0.18-0.26 $\text{Wm}^{-1}\text{K}^{-1}$
243 [28], [63]. From Figure 2, we find that the calculated temperatures (ΔT_{v-av}) using k_{eff} of 0.18
244 $\text{Wm}^{-1}\text{K}^{-1}$ and 0.26 $\text{Wm}^{-1}\text{K}^{-1}$ are indistinguishable from the calculated ΔT_{v-av} for a cuboidal
245 resistance network with $k_{med}=0.58 \text{ Wm}^{-1}\text{K}^{-1}$, R_s'' of 2×10^{-4} and $10^{-4} \text{ K.m}^2\text{W}^{-1}$, respectively. In
246 other words, a $k_{eff}= 0.18-0.26 \text{ Wm}^{-1}\text{K}^{-1}$ that was previously measured for adipose tissues is
247 equivalent to a tissue made up of cells of $L=50 \mu\text{m}$ each with a $k_{med}=0.58 \text{ Wm}^{-1}\text{K}^{-1}$ and $R_s'' =$
248 $2 \times 10^{-4} - 10^{-4} \text{ K.m}^2\text{W}^{-1}$, respectively, as also estimated by Eqn. (4). Thus, the cuboidal resistance
249 network consisting of k_{med} and R_s'' can capture the effective thermal conductivity approximation
250 at tissue length-scales.

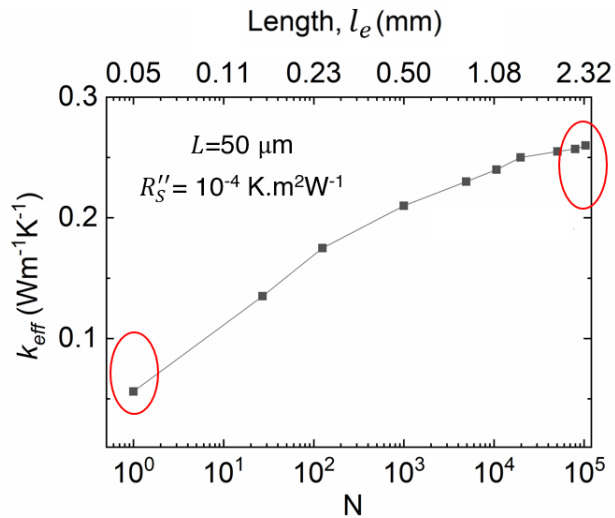
251 At sub-cellular length-scales, a recent report [55] measured the thermal conductivity to be
252 $0.07-0.13 \text{ Wm}^{-1}\text{K}^{-1}$ with a spatial resolution of 200 nm inside a cell. Since the measured k_{eff} is
253 less than protein's thermal conductivity, k_p ($\sim 0.1-0.2 \text{ Wm}^{-1}\text{K}^{-1}$), the interfacial resistances (R_{TIR}'')
254 possibly dominated at sub-cellular length-scales. We approximated the cellular heat diffusion
255 picture to a cuboidal resistance network to explicitly account for the interfacial resistances (R_{TIR}'').
256 Consequently, a low k_{eff} can be explained using the cubic resistance network if the lumped
257 resistance R_s'' is in the range $10^{-7}-10^{-6} \text{ K.m}^2\text{W}^{-1}$ (Figure S2 in supplementary material) at $L \sim 50 \text{ nm}$.
258 Therefore, the cuboidal resistance network can provide a reasonable approximation to the thermal
259 conductivity across a range of sub-cellular to tissue length-scales.

260

261 *Limitations of effective thermal conductivity approximation*

262 The effective thermal conductivity, k_{eff} , is a function of the length-scale at which it was
263 estimated (Figure 3), especially if the local thermal interfacial resistances dominate the total
264 thermal resistance. If the local thermal resistances (R_s'') are in the order of $10^{-4} \text{ K.m}^2\text{W}^{-1}$ at a length-
265 scale of $50 \mu\text{m}$, the effective thermal conductivity is a strong function of the length scale varying
266 from $0.05 \text{ Wm}^{-1}\text{K}^{-1}$ to $0.25 \text{ Wm}^{-1}\text{K}^{-1}$, over $50 \mu\text{m}$ to 2 mm length-scale. Figure 3 shows that the
267 effective thermal conductivity can be as low as $\sim 0.05 \text{ Wm}^{-1}\text{K}^{-1}$ at cellular length-scales ($< 50 \mu\text{m}$),
268 which is in close agreement with a recent report [55] of intracellular k : $0.07-0.13 \text{ Wm}^{-1}\text{K}^{-1}$. We
269 mark this experimentally reported thermal conductivity in red circle in Figure 3 at $N \sim 1$. Similarly,
270 for adipose tissues, the thermal conductivity is typically in the range 0.18-0.26 $\text{Wm}^{-1}\text{K}^{-1}$ [28], [63],
271 which is also highlighted in red in Figure 3 at larger length-scales ($l_e \sim 2 \text{ mm}$). Notably, our
272 resistance network model can capture the thermal conductivity variation from sub-cellular to tissue
273 length-scales. The data shown in black line in Figure 3 corresponds to our specific assumption of
274 a cuboidal topology for the resistance network. In general, the true functional relationship between
275 effective thermal conductivity and length-scale could be determined by mapping the true topology
276 of the resistance network in the system. Our cuboidal topology serves as a generalized example to
277 show that the local interfacial resistances can be responsible for the reduction in effective thermal
278 conductivity at smaller length-scales.

279 The equivalent resistance (R''_s) is responsible for reducing the effective thermal
 280 conductivity at lower length-scales (Figure S2). The value of this resistance R''_s scales directly with
 281 the length-scale (L), as evident from Eqn. (4). A resistance, R''_s , of $\sim 10^{-4}$ K.m²W⁻¹ at a length-scale
 282 $L=50$ μ m may seem high; however, it scales down to an equivalent resistance, R''_s of $\sim 10^{-7}$ K.m²W⁻¹
 283 at a length-scale $L=50$ nm, where the contribution of R''_{TIR_i} can no longer be ignored in R''_s . A
 284 resistance of 10^{-7} K.m²W⁻¹ is comparable to that of hydrophobic-water interfaces [33], [34]. At
 285 sub-cellular length scales ~ 50 nm, if the local resistance R''_s is on the order of 10^{-7} K.m²W⁻¹, k_{eff}
 286 can vary from 0.05 Wm⁻¹K⁻¹ to 0.25 Wm⁻¹K⁻¹ over length scales of 50 nm to 2 μ m (Figure 3). The
 287 interfacial resistance (R''_{TIR}) contribution to the lumped resistance R''_s cannot be ignored at a length-
 288 scale l_e where $R''_s \sim \sum_i R_{TIR_i} \sim l_e/k_p$ could be all in similar orders of magnitude. The exact length-
 289 scale l_e at which R''_{TIR} dominates cannot be known for certain since we do not have any information
 290 on the TIR of multiple interacting protein chains or organelles.



291

292 Figure 3. Effective thermal conductivity (k_{eff}) is a function of the length-scale at which it is measured.
 293 We find the k_{eff} at each length scale, l_e , by matching the volume averaged temperature (T_{v-av}) for a
 294 stack of N cells with a resistance network of k_{med} and R''_s to that of a stack with a k_{eff} . We assumed a
 295 constant volumetric heat of dissipation per cell. The region in red corresponds to some of the previous
 296 experimental data points [28], [55], [63].

297

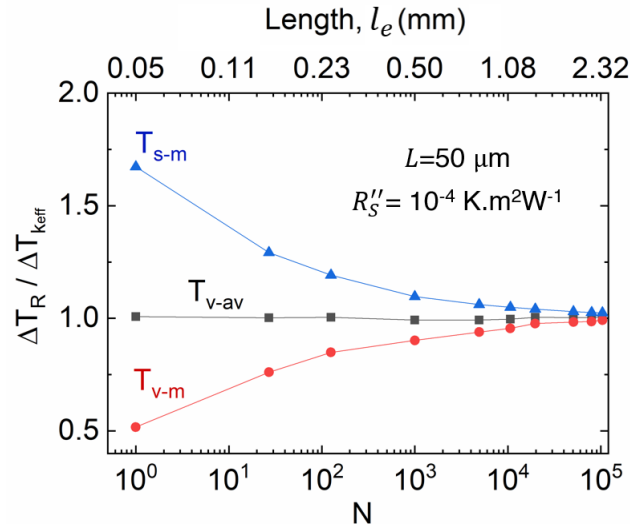
298 The effective thermal conductivity, k_{eff} , is also dependent on the type of input heat source
 299 (volumetric or surface), and the location of the measured temperature. For bioenergetics studies,
 300 we assumed that a k_{eff} is typically measured using the average temperature change over a volume
 301 (ΔT_{v-av}) for a known volumetric heat input, Q . However, if the length-scale l_e of effective thermal
 302 conductivity k_{eff} measurement is in the order of L , which is the length-scale of local resistances
 303 (R''_s), the k_{eff} approximation may fail to capture the true temperature distribution, as shown in
 304 Figure 4. If k_{eff} is used, we denote the temperature changes as $\Delta T_{k_{eff}}$, calculated using the known
 305 k_{eff} . Similarly, we denote the temperature changes calculated using the cuboidal resistance

306 network (k_{med} and R''_s , Figure 1b) as ΔT_R . We find from Figure 4 that if the effective thermal
 307 conductivity is defined using the average temperature (ΔT_{v-av}), the local surface temperatures
 308 (ΔT_{s-m}) can be higher by 67%, or the overall maximum temperature (ΔT_{v-m}) can be lower by
 309 51% in comparison to the true temperature changes (ΔT_R). Only at length-scales $l_e \gg L$, as shown
 310 in Figure 4, an effective thermal conductivity can capture the true temperature distribution.

311 We note here that we assumed the true temperature change to be ΔT_R (in Figure 4),
 312 corresponding to a cuboidal resistance network, which is one of the many possible topologies. The
 313 real picture could be worse (with entangled resistance network and high interfacial resistances) or
 314 better (with a homogenous dispersion of proteins, low cell packing density, and low interfacial
 315 resistance). The former is more likely since it supports the reduction in the effective thermal
 316 conductivity to values below that of typical proteins (Figure 3).

317 Typical calorimetry techniques [41], [42] for biological cells measure the temperature of
 318 the surrounding medium to estimate the total heat released from a cell. Such techniques inherently
 319 assume an effective thermal conductivity for the cell and the surrounding medium during the
 320 calibration of the thermal resistance of the calorimetry cell using an external heater. We discussed
 321 in this section that the effective thermal conductivity is a function of the location of the heat source,
 322 the location of the measured temperature, and the local interface resistance network (Figure 4).
 323 Since the resistance to heat flow for an external heater may be different in comparison to any
 324 intracellular heat sources, previously reported calorimetry techniques [41], [42] may not be able
 325 to capture the true intracellular heat release via externally measured temperatures.

326



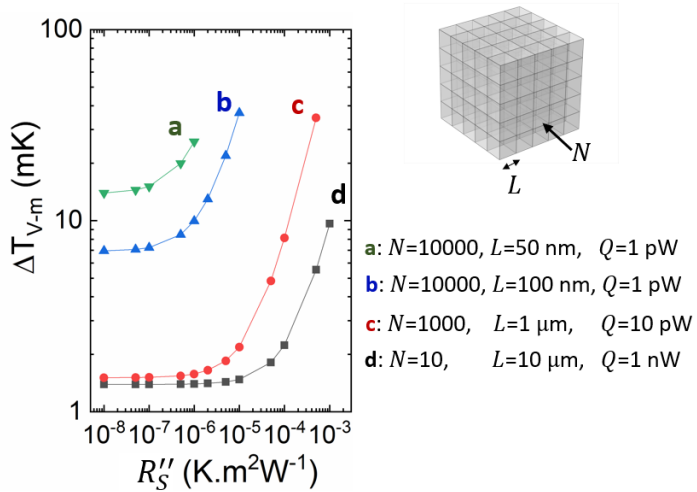
327

328 Figure 4. Effective thermal conductivity (k_{eff}) may not capture the temperature distribution at smaller
 329 length-scales. We use the k_{eff} shown in Figure 3, for this plot. s-m: surface maximum, v-m: volume
 330 maximum, v-av: volume average.

331

332 **Typical temperature changes**

333 In the previous sections, we developed a cuboidal resistance network that offers a generalizable
 334 way to model the interfacial resistances. The topology of the resistance network and the absolute
 335 value of the resistances may vary widely across cell lines. In this section, we explore the typical
 336 endogenous temperature changes for a range of length-scales and interfacial resistances. An
 337 estimate of the typical temperature changes can help determine the required sensitivity of
 338 measurement techniques to measure such temperature changes.



340 Figure 5. Maximum localized temperature changes in sub-cellular compartments due to a total
 341 endogenous heat release rate of 10 nW. We plot this for a range of possible equivalent resistances, R_S'' , at
 342 a length-scale L . The notations a, b, c, d correspond to different types of subcellular compartments. A
 343 conservative thermal conductivity of $0.1 \text{ Wm}^{-1}\text{K}^{-1}$ was assumed for the subcellular compartments and the
 344 surrounding medium (cytosol).

345

346 *Sub-cellular localized temperature changes*

347 In this section, we estimate the localized temperature changes in sub-cellular compartments
 348 due to endogenous heating. Endogenous heat release in individual cells is typically in the range of
 349 $1\text{--}10 \text{ nW}$ in a $50 \mu\text{m}$ diameter cell ($\sim 1\text{--}20 \text{ kW/m}^3$) [28], [41], [62]. We consider a few different
 350 scenarios (listed in Figure 5) each representing different sub-cellular compartment sizes, but all
 351 producing the same 10 nW of total heat. For instance, scenario a has 10,000 compartments each
 352 producing a heat $Q=1 \text{ pW}$ and has a length-scale $L= 50 \text{ nm}$ roughly corresponding to individual
 353 protein chains. On the other hand, the scenario c has 1,000 compartments each producing a heat
 354 $Q=10 \text{ pW}$ and has a length-scale $L= 1 \mu\text{m}$, roughly corresponding to that of mitochondria. In Figure
 355, we show the maximum localized temperature changes in such sub-cellular compartments. We
 356 only plot the temperature changes for a range of possible equivalent resistances R_S'' . For instance,
 357 we do not plot the temperature changes in scenario a for $R_S'' > 10^{-6} \text{ K} \cdot \text{m}^2 \text{W}^{-1}$, since it is unlikely for
 358 protein chains of 50 nm length-scale to have such resistances. The volumetric heat rate for the
 359 scenarios shown in Figure 5 are in the range $\sim 1\text{--} 8000 \text{ MW/m}^3$. Despite such a high volumetric
 360 heat release rate, the localized temperature changes in a cell are expected to be $< 0.1 \text{ K}$. This is

361 contrary to certain previous studies that report intracellular organelles to be ~ 1 K higher than the
362 cytosol [7], [17]. The intracellular temperature changes can be greater than 0.1 K if exogenous
363 stimulants [9], [36], [64], [65] such as proton uncouplers (BAM15, CCCP, FCCP), laser,
364 resonating magnetic nanoparticles, etc. are used to increase the heat released in cells by several
365 orders of magnitude above endogenous conditions. Moreover, transient endogenous temperature
366 fluctuations in a 10 nm sub-cellular compartment can be up to ~ 1 K, but it can only occur over a
367 timescale of 0.1 ns, which could be averaged-out by most measurement techniques [26]. Overall,
368 to measure endogenous and localized temperature changes in intracellular regions, the
369 measurement technique is required to have a detection limit $\ll 100$ mK.

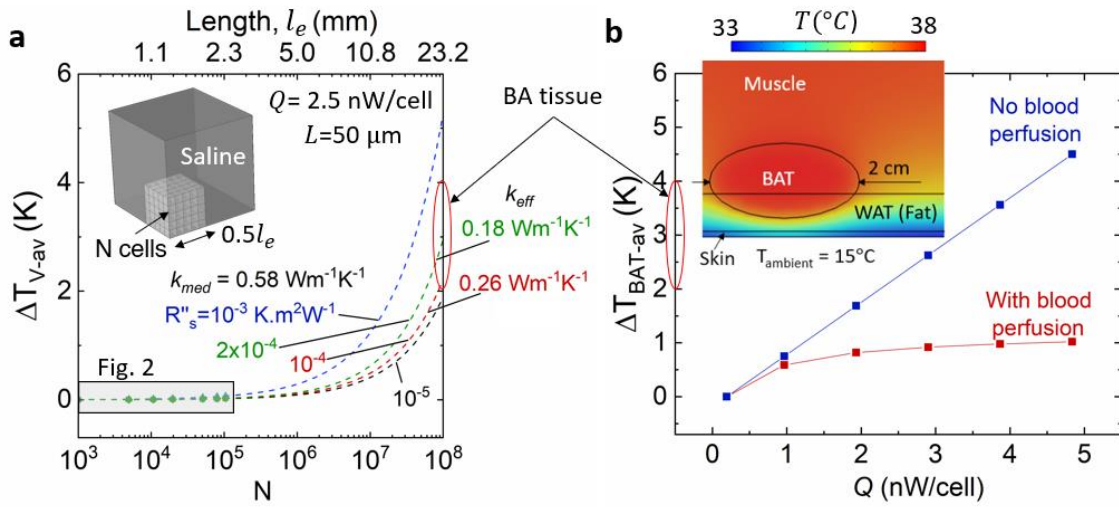
370

371 *Tissue-scale temperature changes*

372 A few nanowatts of intracellular heat cannot raise the local temperature in an isolated cell
373 by a few K as evident from Figure 2 and Figure 5. However, it is well known that brown adipose
374 tissue (BAT) cells contribute toward increasing the local tissue temperatures by 1-2 K [4], [5],
375 especially under cold-induced conditions. In this section, we systematically show how the
376 temperature changes increase from a few mK in a single isolated cell to 1-2 K in tissues through
377 our cuboidal resistance network for cells. We also compare our results against a bioheat transport
378 model that was previously developed for tissues.

379 For a nominal heat of 2.5 nW per cell, we previously discussed in Figure 2 that the average
380 temperature change increases with the number of cells, N . The temperature changes, ΔT_{V-av} , in
381 Figure 2 roughly follows a power-law, $\Delta T_{V-av} \propto N^\gamma$, where $\gamma = 0.63-0.67$, which is consistent
382 with previous analytical estimates [18], [66]. By extrapolating this fit, in Figure 6a, we calculate
383 the corresponding temperature changes at tissue length-scales of ~ 20 mm. The thermal
384 conductivity of adipose tissue is typically in the range of 0.18-0.26 Wm⁻¹K⁻¹. The corresponding
385 ΔT_{V-av} is expected to be in the range of 2-4 K for a tissue of size ~ 20 mm (Figure 6a). We compare
386 this prediction to a 3D bio-heat transport model that was developed for tissues to include the effects
387 of blood perfusion. Details of this model are available in previous studies [27], [28], and also in
388 the supplementary material. Briefly, the bioheat transport model accounts for volumetric metabolic
389 heat production (Q''_{met}) at tissues and blood associated thermoregulation (Q''_{blood}). The blood
390 perfusion rate is expressed as ω_b in s⁻¹. The volumetric heat supplied or removed by the blood is
391 then given by, $Q''_{blood} = \rho_b \omega_b C_b (T_b - T)$, where C_b is the specific heat capacity, ρ_b is the density
392 of the blood, T_b is the arterial blood temperature, and T is the local tissue temperature. In Figure
393 6b, we use the bio-heat transport model to calculate the expected temperature changes in brown
394 adipose tissue (BAT) deposits during a cold-induced ($T_{ambient}=15^\circ\text{C}$) thermogenesis. BAT
395 volumes vary depending on age, location, and weight of the individual. Here, we choose a 2 cm³
396 ellipsoidal BAT as representative of supraclavicular region [28], [67], [68]. We used previously
397 reported thermal and physical properties for blood, fat (BAT and WAT), and muscle, which we
398 also summarize in Table S1 in the supplementary material. Our previous estimation of $\Delta T_{V-av} \sim 2-$
399 4 K rise in a stack of cells (Figure 6a) is equivalent to a scenario in BAT (Figure 6b, $Q=2-3$
400 nW/cell) with no blood perfusion. Notably, we were able to predict the temperature change in
401 tissues by using a framework built from single cells (with k_{med} and R_s'' along a cuboidal resistance

402 network) each producing ~ 2.5 nW of heat. The ΔT from a stack of cells (Figure 6a) did not include
403 the effects of blood transport. Blood perfusion is responsible for the nutrient transport required to
404 sustain the thermogenesis. Considering the effects of blood perfusion, we expect the tissue's
405 temperature to rise by ~ 1 K (Figure 6b). This is also consistent with previous experimental reports
406 that studied thermoregulatory neuronal circuits and report a maximum temperature change in the
407 order of ~ 1 - 2 K in BAT deposits [4], [5]. Even though intracellular temperature changes are $\ll 0.1$
408 K in an isolated cell (~ 50 μ m), the temperature changes can reach 1-2 K at tissue length-scales of
409 ~ 10 mm. Overall, the detection limit required for the measurement of endogenous temperature
410 changes at tissue length-scales are in the order of ~ 0.1 K, which is realizable in common
411 macroscopic measurement techniques.



412
413 Figure 6. a) Average temperature of the stack of cells increases with the number of cells, N , and reaches
414 ~ 2 - 4 K at a length-scale of ~ 20 mm. We extrapolated these curves from Figure 2. b) Average temperature
415 change in the BAT deposit is shown for 5, 10, 15, 20, 25-fold increase in BAT metabolism. The x-axis
416 shows the heat released in the tissue in nW per cell (of dimension 50 μ m x 50 μ m x 50 μ m). The “no
417 blood perfusion” case assumed ω_b to be zero. More details on this bio-heat transport model can be found
418 in the supplementary material.

419
420 **Choosing an appropriate thermometry technique**
421 In the previous section, we estimated the typical endogenous temperature changes at intracellular
422 and tissue length-scales. Such temperature changes occur inherently in the biological medium,
423 irrespective of the measurement technique. When a temperature probe is introduced into the
424 biological milieu, it often measures a temperature that is spatially averaged across the dimensions
425 of the probe [69]. Therefore, in this section, we consider the perspective of the measurement
426 technique and examine the temperature changes measured by the probes employed. Specifically,
427 we consider two commonly used techniques – intracellular and extracellular thermometry. We
428 examine the expected measurement temperatures over a range of cellular to tissue length-scales
429 for biochemical reactions of different timescales and heat rates. Such an analysis would help to

430 identify the optimal thermometry technique that can provide physiological insight for a given type
431 of biochemical reaction.

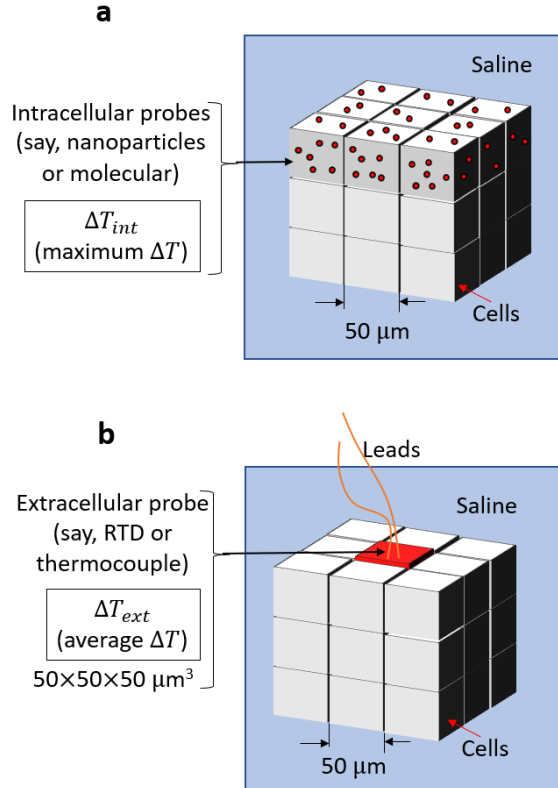
432 Figure 7 schematically depicts the two measurement techniques that we analyze in this
433 section. We define ΔT_{int} as the maximum intracellular temperature that can be measured through
434 infinitesimal intracellular probes (say nanoparticles or molecular probes) dispersed inside the cells
435 at the surface of a tissue of N cells. We define ΔT_{ext} , as the temperature measured by an
436 extracellular probe (say RTD or thermocouple) of $50 \times 50 \times 50 \mu\text{m}^3$ size, which is also assumed to
437 be at the surface of a tissue of N cells. In the following sections, we first analyze the time-scale
438 effects of the measurement temperatures (ΔT_{int} vs. ΔT_{ext}) across a range of length-scales. We then
439 highlight how the temperature changes compare with the typical detectable limits of the
440 measurement techniques.

441

442 *Time-scale effects*

443 We first compare the steady-state temperature changes expected to be measured by extracellular
444 (ΔT_{ext}) and intracellular (ΔT_{int}) probes, as shown in Figure 8. We assume a steady heat release of
445 10 nW per cell of size 50 μm , typical of brown adipose tissue cells under cold-induced
446 thermogenesis. From Figure 8, we find that the ΔT_{ext} and ΔT_{int} closely follow each other on the
447 scale of 0 to 100 mK over a range of length-scales. For $N < 1000$, the absolute magnitude of the
448 temperature changes is < 10 mK, which is lower than the typical detection limits of the
449 measurement techniques. We later discuss (in the following section) the influence of the heat
450 magnitude on the absolute value of the temperatures and how they compare against the detection
451 limit. In Figure 8, we also plot the ratio of the temperature changes, $\Delta T_{int}/\Delta T_{ext}$, which is
452 independent of the absolute magnitude of heat release. The ratio $\Delta T_{int}/\Delta T_{ext}$ reaches a maximum
453 of about 5.8 at $N=1$, which corresponds to an isolated cell. Further, $\Delta T_{int}/\Delta T_{ext}$ remains under 2
454 for $N > 25$ cells. This shows that using an intracellular probe to measure temperature changes is
455 beneficial, especially if the number of cells in the study is less than 10. In other words, intracellular
456 probes can be useful for *in vitro* studies in a petri dish setting, where the temperature changes
457 inside a cell can be up to 5.8 times higher than that outside of a cell, under steady-state conditions.

458

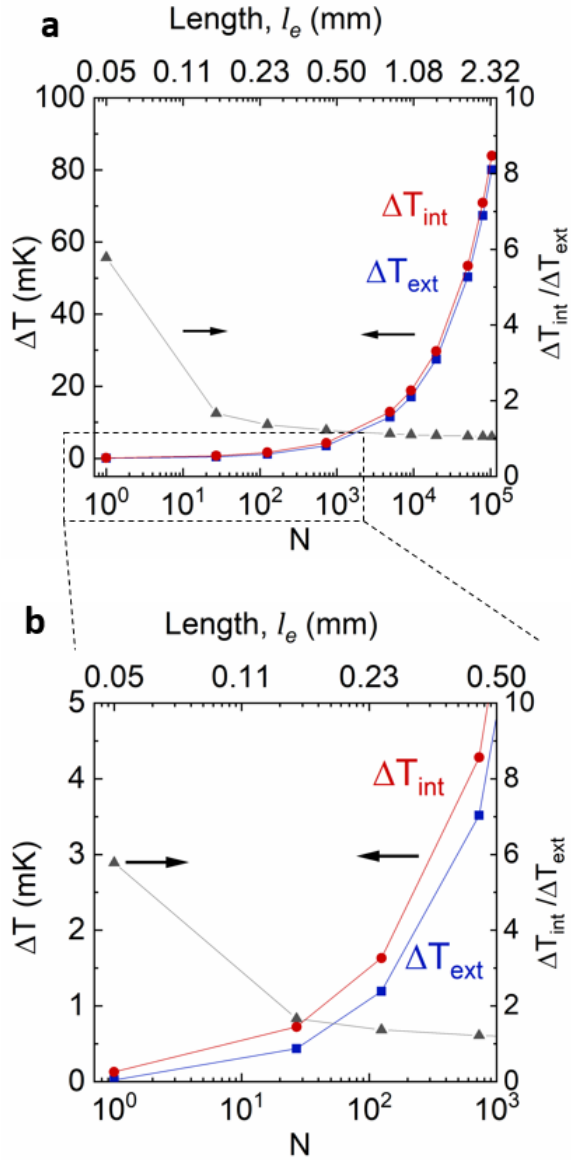


459

460 Figure 7 a) Schematic of intracellular temperature measurement is shown, defining ΔT_{int} as the
 461 maximum intracellular temperature from cells at the surface of N number of cells. b) Schematic of a
 462 typical extracellular temperature measurement is shown, defining ΔT_{ext} as the extracellular temperature
 463 measured at a location of size $(50 \times 50 \times 50 \mu\text{m}^3)$. The probe is assumed to have the same thermal
 464 properties as that of water. We assume a nominal resistance, $R_S'' = 10^{-4} \text{ K.m}^2\text{W}^{-1}$ corresponding to a
 465 $k_{eff} \sim 0.26 \text{ Wm}^{-1}\text{K}^{-1}$.

466

467 Under transient heating conditions, intracellular temperature changes (ΔT_{int}) can be 5-20 times
 468 higher than that measured at extracellular regions (ΔT_{ext}) in an *in vitro* setting for isolated cells.
 469 We depict this in Figure 9, where we show the simulated measurement temperatures for transient
 470 heating of $Q = 10 e^{-t/\tau} \text{nW}$ in a single isolated cell in an infinite medium, releasing heat Q at
 471 different timescales (τ). We find the ratio $\Delta T_{int}/\Delta T_{ext}$ to increase from 5.8 (~for steady-state
 472 conditions) to up to 18 at a timescale of $\tau=1 \text{ ms}$ for the heat release. The ratio $\Delta T_{int}/\Delta T_{ext}$ is high
 473 at lower timescales (τ) primarily because the time taken for the heat to diffuse (given by L^2/α ,
 474 where L is the length-scale and α is the thermal diffusivity) and reach the extracellular probes is
 475 higher than the heat release duration (τ). Thus, the heat is spatially confined to intracellular regions.
 476 Intracellular thermometry is, therefore, better suited in isolated cells *in vitro*, especially if the heat
 477 release is expected to be transient with a timescale $\ll 1 \text{ s}$.

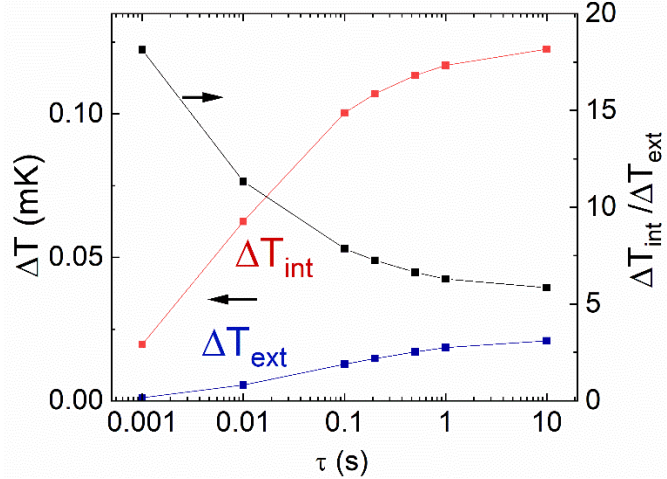


478

479 Figure 8 a) The extracellular (ΔT_{ext} , blue points) and intracellular (ΔT_{int} , red points) temperature changes
 480 during endogenous thermogenesis (10 nW, steady state per cell) are plotted on the left y-axis. The ratio
 481 $\Delta T_{int}/\Delta T_{ext}$ (black points) is plotted on the right y-axis. b) The temperature changes over $N=1$ to 1000 is
 482 plotted separately to clearly show the magnitude of temperature changes at small length-scales. We
 483 assumed the cell to have edge length $L=50$ μm . The ratio $\Delta T_{int}/\Delta T_{ext}$ is independent of the magnitude of
 484 heat.

485

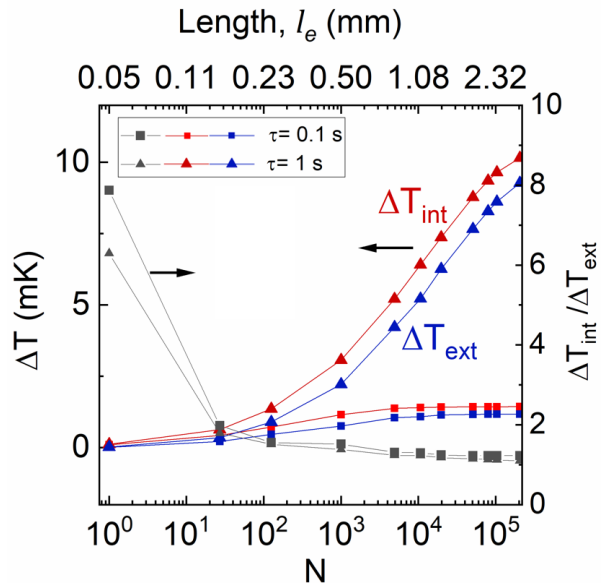
486



487

488 Figure 9: The intracellular (ΔT_{int} , red) and extracellular (ΔT_{ext} , blue) temperature changes are plotted
 489 along the left y-axis for a transient heat release ($10 e^{-t/\tau}$ nW) in an isolated cell in an infinite saline
 490 medium. The ratio $\Delta T_{int}/\Delta T_{ext}$ (black points) is plotted on the right y-axis. The ratio $\Delta T_{int}/\Delta T_{ext}$ is
 491 independent of the magnitude of heat.

492



493

494 Figure 10. The extracellular (ΔT_{ext} , blue points) and intracellular (ΔT_{int} , red points) temperature changes
 495 during transient thermogenesis ($10 e^{-t/\tau}$ nW per cell) are plotted on the left y-axis. The ratio $\Delta T_{int}/\Delta T_{ext}$
 496 (black points) is plotted on the right y-axis. We assumed the cell to have edge length $L=50 \mu\text{m}$ and
 497 $R_S'' \sim 10^{-4} \text{ K.m}^2\text{W}^{-1}$. The ratio $\Delta T_{int}/\Delta T_{ext}$ is independent of the magnitude of heat.

498 Since the transient heating is localized within a cell, the transient temperature changes do
 499 not increase at larger length-scales. In Figure 6 and Figure 8, the steady-state heating resulted in
 500 the corresponding temperature change (ΔT) to increase with the number of cells (N) as $\Delta T \sim N^\gamma$.
 501 However, if the heat release is transient in nature, as shown in Figure 10, the corresponding
 502 temperature changes do not increase with the number of cells (N) beyond a certain N . Moreover,

503 from Figure 10, we find that a smaller timescale of heat release ($\tau \sim 0.1$ s) results in temperature
504 changes that saturate at smaller length-scales ($l_e \sim 1$ mm) than that for $\tau \sim 1$ s. This is expected since
505 the heat diffusion length ($\sqrt{\alpha\tau}$) is smaller for shorter heat release duration (τ). Overall, we again
506 find that intracellular thermometry is better suited for transiently thermogenic reactions with
507 timescales $\ll 1$ s in isolated cells under *in vitro* conditions; however, at larger length-scales,
508 extracellular thermometry is also equally suited to measure the temperature changes since
509 $\Delta T_{int}/\Delta T_{ext} \rightarrow 1$ for length-scales $l_e > 0.2$ mm. Throughout this section, we analyzed the ratio
510 $\Delta T_{int}/\Delta T_{ext}$ to conclude that intracellular thermometry is better suited for transients in isolated
511 cells; however, the absolute magnitude of ΔT_{int} is < 1 mK (Figures 8-10) in isolated cells, which
512 renders it not possible to measure using conventional techniques. We discuss the implications of
513 the absolute temperature changes and the heat rate magnitudes in the following section.

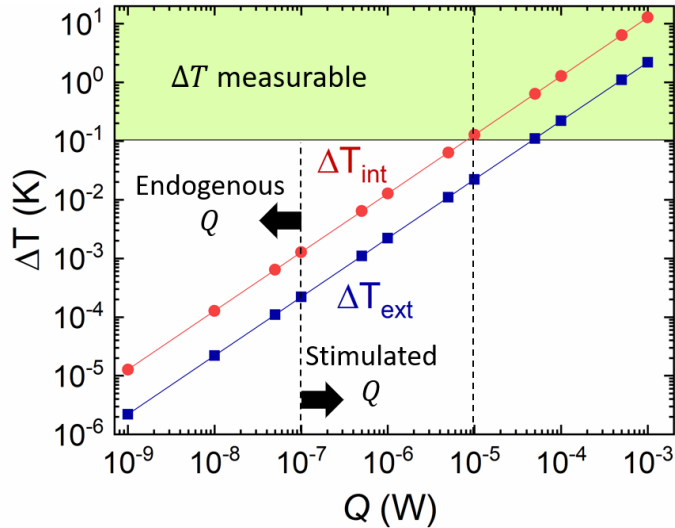
514

515 *Heat rate magnitude: endogenous vs stimulated*

516 Under physiological conditions, intracellular temperature changes are usually limited to
517 sub-mK values, which are not directly measurable *in vitro* by intracellular probes, unless the cells
518 are thermally isolated by multiple vacuum chambers [41], [42]. However, if the intracellular heat
519 release can be stimulated by external agents, the intracellular temperature changes can reach
520 measurable limits, as we show in Figure 11. We plot the steady-state temperature changes (ΔT_{int}
521 and ΔT_{ext}) in an isolated cell in a petri dish setting, for a range of uniform volumetric heat release
522 Q inside the cell. Typically, any physiological heat release rate is < 100 nW [28], [41], [42], [62]
523 as marked in Figure 11. To increase the expected temperatures to measurable limits
524 (conservatively, 0.1 K), the intracellular heat release needs to be stimulated exogenously to > 10
525 μ W. Stimulated mitochondrial proton uncoupling [9] is one such example, where the heat release
526 is stimulated by an external proton uncoupler. Other examples of exogenous heating include laser
527 [65], resonating magnetic nanoparticles [36], norepinephrine [64], etc. Only when the intracellular
528 heat release is stimulated, intracellular thermometry techniques can provide useful and measurable
529 physiological information on the stimulated biochemical reaction. Therefore, intracellular
530 temperature probes can be useful for steady-state and transient measurements *in vitro*, especially
531 if the intracellular heat release is stimulated exogenously.

532 On the other hand, extracellular thermometry can be useful for probing endogenously
533 thermogenic reactions at tissue length-scales. The steady-state temperature changes increase with
534 the length-scale and reach up to a few K at $l_e \sim 10$ mm, as evident from Figure 6. At such length-
535 scales ($l_e > 10$ mm), the extracellular probe can directly measure thermogenesis-induced
536 temperature changes. Further, there is little benefit to using intracellular probes at larger length-
537 scales (> 1 mm) as evident from Figure 8a. Therefore, extracellular temperature probes can provide
538 useful physiological information on endogenous thermogenesis-related activities at larger length-
539 scales such as tissues/organs that are > 1 mm. This is also evident from previous studies that
540 utilized mm-scale thermometers to study thermoregulatory neuronal circuits [4], [5], and cancer
541 metabolism [6], [29], [70], [71].

542



543

544 Figure 11. For a single isolated cell in a typical petri dish setting, the intracellular (ΔT_{int} , red) and
 545 extracellular (ΔT_{ext} , blue) temperature changes are plotted for various steady-state volumetric heat release
 546 rates, Q . Physiologically expected heat release rates are $\ll 100$ nW. The typical intracellular temperature
 547 measurement limit is > 0.1 K, in an *in vitro* petri dish setting.

548

549 **SUMMARY OF DISCUSSION**

550 In the discussions above, we explained how our heat diffusion model can be used to design
 551 cellular thermometry experiments. Here, we first summarize our key recommendations, provide
 552 relevant examples, and then address some limitations. We explored different thermometry options
 553 and thermogenic reactions of different heat rates and times-scales to identify which technique is
 554 optimal for a given reaction. By investigating a range of parameters such as length-scales,
 555 timescales, and expected heat release rates, we find the following:

556 1. Intracellular thermometry is useful in a petri dish setting for *in vitro* studies, especially if
 557 the intracellular heat release is stimulated exogenously and is transient in nature occurring
 558 over < 1 s. For instance, a previous study utilized a nanodiamond-based intracellular
 559 thermometer and laser-induced heating to find that the early embryonic development in *C. elegans*
 560 is determined independently by individual cells rather than cell-to-cell
 561 communications [72]. Another study utilized a microfabricated intracellular thermometer
 562 in *Aplysia* neurons and observed transient heating during sudden mitochondrial
 563 depolarization by proton uncoupler BAM15 [9]. Such intracellular thermometry studies
 564 utilizing exogenous stimulants can result in temperature changes above detection limits
 565 and provide unprecedented insights into the subcellular metabolic pathways.

566 2. Extracellular thermometry is useful to observe physiologically relevant and endogenous
 567 thermogenesis, especially in tissues (> 1 mm length-scale). For instance, a previous study
 568 utilized an extracellular thermistor probe to observe that the brown adipose tissue (BAT)
 569 thermogenesis is controlled by a synergy between Leptin and thyrotropin-releasing

570 hormone in the rat's hindbrain [5]. Another study observed that the hypothalamic orexin-
571 synthesizing neurons contribute to the intensity with which rats respond to external
572 conditions, by measuring BAT temperatures through a thermistor [73]. Since the
573 endogenous temperature changes in tissues [1], [2], [6] can be above the detection limits,
574 they can provide direct insights into the metabolic pathways being probed.

575 Other non-conventional thermometry techniques such as isolating a cell in a microfluidic
576 channel or micropipettes with multiple isothermal vacuum chambers have been previously
577 attempted [41], [42]. Such techniques increase the resistance to heat flow, which can increase the
578 temperature changes above detection limits even for a nominal endogenous heat release \sim 1-10 nW
579 from one or few cells. However, under such isolated conditions, transient temperature
580 measurements in the order of sub-seconds are yet to be developed. Overall, future bioenergetics
581 studies can choose an appropriate thermometry technique using our guidelines discussed here, if
582 the underlying biochemical reaction's timescale and stimulation mechanisms are known.

583 Throughout this work, we utilized a cellular heat diffusion model with a cuboidal network
584 of resistance R''_s to capture the influence of interfacial resistances in the cellular milieu. We
585 assumed a constant k_{med} of $0.58 \text{ W m}^{-1} \text{ K}^{-1}$ corresponding to water (k_{water}) and concentrated all
586 the resistances from the proteins or organelles to be at R''_s . However, cellular heat diffusion could
587 be from a combination of k_{med} ($< k_{water}$, due to a homogeneous distribution of proteins and ions
588 or low packing density) and R''_s , where the magnitude of $R''_s (= \sum_i R_{TIR_i})$ could be less than that
589 used throughout this work. Similarly, the increase in thermal conductivity at large length-scales
590 could be due to a low packing density of cells in tissues. Further, lipid bilayers and other proteins
591 undergo phase change near room temperatures [74], [75], which may influence the local thermal
592 resistances. Thus, the effective thermal conductivity (k_{eff}) may likely depend not only on the
593 length-scale but also on the temperature at which they are measured. Future intracellular
594 thermometry studies can provide insights on the length-scale and temperature dependence of
595 thermal properties (k_{eff} and R''_s) by measuring the local temperature changes across a range of
596 length-scales $50 \text{ nm} - 100 \mu\text{m}$ using a certain heat input. Spatial distribution of the local thermal
597 interfacial resistances can be known if spatial temperature distributions can also be measured
598 across the cellular medium. Recent studies [59], [76] have measured the thermal properties of the
599 lipid bilayers in cell membranes; however, measurements on cytoskeleton components such as
600 actin, microtubules, intermediate filaments, etc. are necessary to understand the significance of
601 their thermal interfacial resistance. Additional topographical information on the biomolecular
602 interfaces and their interface resistance values may help to improve the heat diffusion model.
603 Nonetheless, the cuboidal resistance network used in this work served as a generalized example to
604 understand the influence of the interface resistances.

605 CONCLUSION

606 In conclusion, our work provides recommendations on choosing a thermometry technique
607 by quantifying whether/when temperature changes are measurable under different biological
608 conditions. A cellular heat diffusion model that incorporates the effects of dissimilar interfaces,
609 provides the temperatures estimated in this work. We show that the commonly used effective

610 thermal conductivity parameter may fail to capture true temperature distributions in the cellular
611 milieu. This is particularly true at sub-cellular length scales where local interfacial resistances can
612 be in the order of 10^{-7} - 10^{-6} K.m²W⁻¹, which can result in an effective thermal conductivity (k_{eff})
613 substantially lower than those of the medium (k_{med}) and proteins (k_p). We captured the reduction
614 in thermal conductivity at lower length-scales, as a test case, using a cuboidal topology for the
615 interfacial resistance network. Our results underscore the need for future studies to measure and
616 map the thermal interfacial resistances in the cellular medium. Further, we find that in subcellular
617 organelles, temperature changes are expected to be less than 100 mK under physiological
618 conditions. In contrast, at tissue scales, we find that even endogenous heat of few nanowatts per
619 cell can produce 1-2 K overall temperature change, which is typical in cold-induced
620 thermogenesis. Thus, extracellular probes are better suited to probing endogenous thermogenic
621 reactions, since the temperature changes exceed detection limits at tissue length-scales. On the
622 other hand, intracellular thermometry is better suited to probing transient thermogenic reactions
623 since transient temperature changes are typically localized within the cell. However, such
624 intracellular temperature changes are measurable only if the biochemical reaction is stimulated
625 exogenously. Overall, this work provides insight into cellular heat diffusion modeling, using which
626 we show how to choose the right thermometry technique to probe a biochemical pathway.

627

628 **Supplementary material:**

629 A supplementary material document accompanies this paper.

630

631 **Acknowledgments:**

632 We thank Dr. Jeffrey Brown, Prof. Daniel Llano, and Prof. Rhanor Gillette for their useful inputs
633 throughout this work. Figure 1 was made in part using biorender.com. This work was supported
634 in part by funding from the National Science Foundation through Grant No. NSF-CBET-17-
635 06854.

636

637 **Supporting citations:**

638 References [77-83] appear in the supplementary material.

639

640 **References:**

641 [1] U. R. Acharya, E. Y. K. Ng, J.-H. Tan, and S. V. Sree, “Thermography based breast cancer
642 detection using texture features and Support Vector Machine,” *J Med Syst*, vol. 36, no. 3,
643 Art. no. 3, Jun. 2012, doi: 10.1007/s10916-010-9611-z.

644 [2] A. Helmy, M. Holdmann, and M. Rizkalla, “Application of thermography for non-invasive
645 diagnosis of thyroid gland disease,” *IEEE Trans Biomed Eng*, vol. 55, no. 3, Art. no. 3,
646 Mar. 2008, doi: 10.1109/TBME.2008.915731.

647 [3] C. Guy, F. Kaplan, J. Kopka, J. Selbig, and D. K. Hincha, “Metabolomics of temperature
648 stress,” *Physiol Plant*, vol. 132, no. 2, Art. no. 2, Feb. 2008, doi: 10.1111/j.1399-
649 3054.2007.00999.x.

650 [4] S. F. Morrison, C. J. Madden, and D. Tupone, “Central Neural Regulation of Brown
651 Adipose Tissue Thermogenesis and Energy Expenditure,” *Cell Metabolism*, vol. 19, no. 5,
652 pp. 741–756, May 2014, doi: 10.1016/j.cmet.2014.02.007.

653 [5] R. C. Rogers, M. J. Barnes, and G. E. Hermann, “Leptin ‘gates’ thermogenic action of
654 thyrotropin-releasing hormone in the hindbrain,” *Brain Research*, vol. 1295, pp. 135–141,
655 Oct. 2009, doi: 10.1016/j.brainres.2009.07.063.

656 [6] P. M. Gullino, R. K. Jain, and F. H. Grantham, “Temperature Gradients and Local
657 Perfusion in a Mammary Carcinoma,” *J Natl Cancer Inst*, vol. 68, no. 3, pp. 519–533, Mar.
658 1982, doi: 10.1093/jnci/68.3.519.

659 [7] K. Okabe, N. Inada, C. Gota, Y. Harada, T. Funatsu, and S. Uchiyama, “Intracellular
660 temperature mapping with a fluorescent polymeric thermometer and fluorescence lifetime
661 imaging microscopy,” *Nat Commun*, vol. 3, p. 705, Feb. 2012, doi: 10.1038/ncomms1714.

662 [8] S. Kiyonaka *et al.*, “Genetically encoded fluorescent thermosensors visualize subcellular
663 thermoregulation in living cells,” *Nat. Methods*, vol. 10, no. 12, Art. no. 12, Dec. 2013, doi:
664 10.1038/nmeth.2690.

665 [9] M. C. Rajagopal *et al.*, “Transient heat release during induced mitochondrial proton
666 uncoupling,” *Communications Biology*, vol. 2, no. 1, Art. no. 1, Jul. 2019, doi:
667 10.1038/s42003-019-0535-y.

668 [10] J. Zhou, B. del Rosal, D. Jaque, S. Uchiyama, and D. Jin, “Advances and challenges for
669 fluorescence nanothermometry,” *Nature Methods*, vol. 17, no. 10, Art. no. 10, Oct. 2020,
670 doi: 10.1038/s41592-020-0957-y.

671 [11] R. Tanimoto *et al.*, “Detection of Temperature Difference in Neuronal Cells,” *Scientific
672 reports*, vol. 6, p. 22071, Mar. 2016, doi: 10.1038/srep22071.

673 [12] T. Tsuji, K. Ikado, H. Koizumi, S. Uchiyama, and K. Kajimoto, “Difference in intracellular
674 temperature rise between matured and precursor brown adipocytes in response to uncoupler
675 and β -adrenergic agonist stimuli,” *Scientific Reports*, vol. 7, no. 1, Art. no. 1, Oct. 2017,
676 doi: 10.1038/s41598-017-12634-7.

677 [13] W. Tian *et al.*, “A high precision apparatus for intracellular thermal response at single-cell
678 level,” *Nanotechnology*, vol. 26, no. 35, Art. no. 35, Aug. 2015, doi: 10.1088/0957-
679 4484/26/35/355501.

680 [14] C. Wang *et al.*, “Determining intracellular temperature at single-cell level by a novel
681 thermocouple method,” *Cell Res.*, vol. 21, no. 10, Art. no. 10, Oct. 2011, doi:
682 10.1038/cr.2011.117.

683 [15] S. Arai, S.-C. Lee, D. Zhai, M. Suzuki, and Y. T. Chang, “A Molecular Fluorescent Probe
684 for Targeted Visualization of Temperature at the Endoplasmic Reticulum,” *Scientific
685 Reports*, vol. 4, no. 1, Art. no. 1, Oct. 2014, doi: 10.1038/srep06701.

686 [16] Y. Takei *et al.*, “A Nanoparticle-Based Ratiometric and Self-Calibrated Fluorescent
687 Thermometer for Single Living Cells,” *ACS Nano*, vol. 8, no. 1, pp. 198–206, Jan. 2014,
688 doi: 10.1021/nn405456e.

689 [17] D. Chrétien *et al.*, “Mitochondria are physiologically maintained at close to 50 °C,” *PLOS*
690 *Biology*, vol. 16, no. 1, p. e2003992, Jan. 2018, doi: 10.1371/journal.pbio.2003992.

691 [18] G. Baffou, H. Rigneault, D. Marguet, and L. Jullien, “A critique of methods for temperature
692 imaging in single cells,” *Nat. Methods*, vol. 11, no. 9, Art. no. 9, Sep. 2014, doi:
693 10.1038/nmeth.3073.

694 [19] G. Baffou, H. Rigneault, D. Marguet, and L. Jullien, “Reply to: ‘Validating subcellular
695 thermal changes revealed by fluorescent thermosensors’ and ‘The 10 5 gap issue between
696 calculation and measurement in single-cell thermometry,’” *Nature Methods*, vol. 12, no. 9,
697 Art. no. 9, Sep. 2015, doi: 10.1038/nmeth.3552.

698 [20] S. Kiyonaka, R. Sakaguchi, I. Hamachi, T. Morii, T. Yoshizaki, and Y. Mori, “Validating
699 subcellular thermal changes revealed by fluorescent thermosensors,” *Nature Methods*, vol.
700 12, no. 9, Art. no. 9, Sep. 2015, doi: 10.1038/nmeth.3548.

701 [21] M. Suzuki, V. Zeeb, S. Arai, K. Oyama, and S. Ishiwata, “The 105 gap issue between
702 calculation and measurement in single-cell thermometry,” *Nat Methods*, vol. 12, no. 9, Art.
703 no. 9, Sep. 2015, doi: 10.1038/nmeth.3551.

704 [22] A. D. Pickel, A. Teitelboim, E. M. Chan, N. J. Borys, P. J. Schuck, and C. Dames,
705 “Apparent self-heating of individual upconverting nanoparticle thermometers,” *Nature
706 Communications*, vol. 9, no. 1, Art. no. 1, Nov. 2018, doi: 10.1038/s41467-018-07361-0.

707 [23] A. Vyšniauskas, M. Qurashi, N. Gallop, M. Balaz, H. L. Anderson, and M. K. Kuimova,
708 “Unravelling the effect of temperature on viscosity-sensitive fluorescent molecular rotors,”
709 *Chemical Science*, vol. 6, no. 10, pp. 5773–5778, 2015, doi: 10.1039/C5SC02248G.

710 [24] D. Chrétien *et al.*, “Pitfalls in Monitoring Mitochondrial Temperature Using Charged
711 Thermosensitive Fluorophores,” *Chemosensors*, vol. 8, no. 4, Art. no. 4, Dec. 2020, doi:
712 10.3390/chemosensors8040124.

713 [25] G. Baffou, I. Bordacchini, A. Baldi, and R. Quidant, “Simple experimental procedures to
714 distinguish photothermal from hot-carrier processes in plasmonics,” *Light: Science &
715 Applications*, vol. 9, no. 1, Art. no. 1, Jun. 2020, doi: 10.1038/s41377-020-00345-0.

716 [26] M. Suzuki and T. Plakhotnik, “The challenge of intracellular temperature,” *Biophys Rev*,
717 vol. 12, no. 2, pp. 593–600, Apr. 2020, doi: 10.1007/s12551-020-00683-8.

718 [27] J. Crezee and J. J. W. Lagendijk, “Experimental verification of bioheat transfer theories:
719 measurement of temperature profiles around large artificial vessels in perfused tissue,”
720 *Phys. Med. Biol.*, vol. 35, no. 7, pp. 905–923, Jul. 1990, doi: 10.1088/0031-9155/35/7/007.

721 [28] D. B. Rodrigues *et al.*, “Numerical 3D modeling of heat transfer in human tissues for
722 microwave radiometry monitoring of brown fat metabolism,” *Proc SPIE*, vol. 8584, Feb.
723 2013, doi: 10.1117/12.2004931.

724 [29] R. K. Jain, F. H. Grantham, and P. M. Gullino, “Blood Flow and Heat Transfer in Walker
725 256 Mammary Carcinoma,” *J Natl Cancer Inst*, vol. 62, no. 4, pp. 927–933, Apr. 1979, doi:
726 10.1093/jnci/62.4.927.

727 [30] P. Kapitza, “The study of heat transfer in helium II,” *J. Phys. (Moscow)*, vol. 4, p. 181,
728 1941.

729 [31] Z. Ge, D. G. Cahill, and P. V. Braun, “AuPd Metal Nanoparticles as Probes of Nanoscale
730 Thermal Transport in Aqueous Solution,” *J. Phys. Chem. B*, vol. 108, no. 49, pp. 18870–
731 18875, Dec. 2004, doi: 10.1021/jp048375k.

732 [32] O. M. Wilson, X. Hu, D. G. Cahill, and P. V. Braun, “Colloidal metal particles as probes of
733 nanoscale thermal transport in fluids,” *Phys. Rev. B*, vol. 66, no. 22, p. 224301, Dec. 2002,
734 doi: 10.1103/PhysRevB.66.224301.

735 [33] Z. Ge, D. G. Cahill, and P. V. Braun, "Thermal Conductance of Hydrophilic and
736 Hydrophobic Interfaces," *Phys. Rev. Lett.*, vol. 96, no. 18, p. 186101, May 2006, doi:
737 10.1103/PhysRevLett.96.186101.

738 [34] H. M. Duong, D. V. Papavassiliou, K. J. Mullen, B. L. Wardle, and S. Maruyama, "A
739 numerical study on the effective thermal conductivity of biological fluids containing single-
740 walled carbon nanotubes," *International Journal of Heat and Mass Transfer*, vol. 52, no.
741 23, pp. 5591–5597, Nov. 2009, doi: 10.1016/j.ijheatmasstransfer.2009.06.016.

742 [35] K. Khosla, L. Zhan, A. Bhati, A. Carley-Clopton, M. Hagedorn, and J. Bischof,
743 "Characterization of Laser Gold Nanowarming: A Platform for Millimeter-Scale
744 Cryopreservation," *Langmuir*, vol. 35, no. 23, pp. 7364–7375, Jun. 2019, doi:
745 10.1021/acs.langmuir.8b03011.

746 [36] N. Manuchehrabadi *et al.*, "Improved tissue cryopreservation using inductive heating of
747 magnetic nanoparticles," *Science Translational Medicine*, vol. 9, no. 379, Mar. 2017, doi:
748 10.1126/scitranslmed.aah4586.

749 [37] E. M. Knavel and C. L. Brace, "Tumor Ablation: Common Modalities and General
750 Practices," *Tech Vasc Interv Radiol*, vol. 16, no. 4, pp. 192–200, Dec. 2013, doi:
751 10.1053/j.tvir.2013.08.002.

752 [38] G. Poggi, N. Tosoratti, B. Montagna, and C. Picchi, "Microwave ablation of hepatocellular
753 carcinoma," *World J Hepatol*, vol. 7, no. 25, pp. 2578–2589, Nov. 2015, doi:
754 10.4254/wjh.v7.i25.2578.

755 [39] D. Li, J. Kang, B. J. Golas, V. W. Yeung, and D. C. Madoff, "Minimally invasive local
756 therapies for liver cancer," *Cancer Biol Med*, vol. 11, no. 4, pp. 217–236, Dec. 2014, doi:
757 10.7497/j.issn.2095-3941.2014.04.001.

758 [40] M. C. Rajagopal, K. V. Valavala, D. Gelda, J. Ma, and S. Sinha, "Fabrication and
759 characterization of thermocouple probe for use in intracellular thermometry," *Sensors and
760 Actuators A: Physical*, vol. 272, pp. 253–258, Apr. 2018, doi: 10.1016/j.sna.2018.02.004.

761 [41] S. Hong *et al.*, "Sub-nanowatt microfluidic single-cell calorimetry," *Nature
762 Communications*, vol. 11, no. 1, Art. no. 1, Jun. 2020, doi: 10.1038/s41467-020-16697-5.

763 [42] S. Hur, R. Mittapally, S. Yadlapalli, P. Reddy, and E. Meyhofer, "Sub-nanowatt resolution
764 direct calorimetry for probing real-time metabolic activity of individual *C. elegans* worms,"
765 *Nature Communications*, vol. 11, no. 1, Art. no. 1, Jun. 2020, doi: 10.1038/s41467-020-
766 16690-y.

767 [43] A. S. Verkman, "Solute and macromolecule diffusion in cellular aqueous compartments,"
768 *Trends in Biochemical Sciences*, vol. 27, no. 1, pp. 27–33, Jan. 2002, doi: 10.1016/S0968-
769 0004(01)02003-5.

770 [44] G. Chen, "Ballistic-Diffusive Heat-Conduction Equations," *Phys. Rev. Lett.*, vol. 86, no. 11,
771 pp. 2297–2300, Mar. 2001, doi: 10.1103/PhysRevLett.86.2297.

772 [45] C. Chen, Z. Du, and L. Pan, "Extending the diffusion approximation to the boundary using
773 an integrated diffusion model," *AIP Advances*, vol. 5, no. 6, p. 067115, Jun. 2015, doi:
774 10.1063/1.4922269.

775 [46] G. Balasubramanian and I. K. Puri, "Heat conduction across a solid-solid interface:
776 Understanding nanoscale interfacial effects on thermal resistance," *Appl. Phys. Lett.*, vol.
777 99, no. 1, p. 013116, Jul. 2011, doi: 10.1063/1.3607477.

778 [47] B. H. Kim, A. Beskok, and T. Cagin, "Molecular dynamics simulations of thermal
779 resistance at the liquid-solid interface," *J. Chem. Phys.*, vol. 129, no. 17, p. 174701, Nov.
780 2008, doi: 10.1063/1.3001926.

781 [48] A. Rajabpour, R. Seif, S. Arabha, M. M. Heyhat, S. Merabia, and A. Hassanali, “Thermal
782 transport at a nanoparticle-water interface: A molecular dynamics and continuum modeling
783 study,” *J. Chem. Phys.*, vol. 150, no. 11, p. 114701, Mar. 2019, doi: 10.1063/1.5084234.
784 [49] Y. Wang and P. Kebinski, “Role of wetting and nanoscale roughness on thermal
785 conductance at liquid-solid interface,” *Appl. Phys. Lett.*, vol. 99, no. 7, p. 073112, Aug.
786 2011, doi: 10.1063/1.3626850.
787 [50] L. Xue, P. Kebinski, S. R. Phillpot, S. U.-S. Choi, and J. A. Eastman, “Effect of liquid
788 layering at the liquid–solid interface on thermal transport,” *International Journal of Heat
789 and Mass Transfer*, vol. 47, no. 19, pp. 4277–4284, Sep. 2004, doi:
790 10.1016/j.ijheatmasstransfer.2004.05.016.
791 [51] J.-L. BARRAT and F. CHIARUTTINI, “Kapitza resistance at the liquid–solid interface,”
792 *Molecular Physics*, vol. 101, no. 11, pp. 1605–1610, Jun. 2003, doi:
793 10.1080/0026897031000068578.
794 [52] A. Lervik, F. Bresme, and S. Kjelstrup, “Heat transfer in soft nanoscale interfaces: the
795 influence of interface curvature,” *Soft Matter*, vol. 5, no. 12, pp. 2407–2414, 2009, doi:
796 10.1039/B817666C.
797 [53] A. Lervik, F. Bresme, S. Kjelstrup, D. Bedeaux, and J. M. Rubi, “Heat transfer in protein –
798 water interfaces,” *Physical Chemistry Chemical Physics*, vol. 12, no. 7, pp. 1610–1617,
799 2010, doi: 10.1039/B918607G.
800 [54] M. C. Rajagopal, T. Man, A. Agrawal, G. Kuntumalla, and S. Sinha, “Intrinsic thermal
801 interfacial resistance measurement in bonded metal–polymer foils,” *Review of Scientific
802 Instruments*, vol. 91, no. 10, p. 104901, Oct. 2020, doi: 10.1063/5.0012404.
803 [55] S. Sotoma *et al.*, “In situ measurement of intracellular thermal conductivity using heater-
804 thermometer hybrid diamond nanosensor,” *bioRxiv*, p. 2020.06.03.126789, Jun. 2020, doi:
805 10.1101/2020.06.03.126789.
806 [56] M. P. Clausen, H. Colin-York, F. Schneider, C. Eggeling, and M. Fritzsche, “Dissecting the
807 actin cortex density and membrane-cortex distance in living cells by super-resolution
808 microscopy,” *J. Phys. D: Appl. Phys.*, vol. 50, no. 6, p. 064002, Jan. 2017, doi:
809 10.1088/1361-6463/aa52a1.
810 [57] C. M. O’Connor, J. U. Adams, and J. Fairman, “Essentials of cell biology,” *Cambridge,
811 MA: NPG Education*, vol. 1, p. 54, 2010.
812 [58] H. C. Chang *et al.*, “Composite Structured Surfaces for Durable Dropwise Condensation,”
813 *International Journal of Heat and Mass Transfer*, vol. 156, p. 119890, Aug. 2020, doi:
814 10.1016/j.ijheatmasstransfer.2020.119890.
815 [59] A. R. N. Bastos *et al.*, “Thermal Properties of Lipid Bilayers Determined Using
816 Upconversion Nanothermometry,” *Advanced Functional Materials*, vol. 29, no. 48, p.
817 1905474, 2019, doi: 10.1002/adfm.201905474.
818 [60] C. E. Hagberg *et al.*, “Flow Cytometry of Mouse and Human Adipocytes for the Analysis
819 of Browning and Cellular Heterogeneity,” *Cell Reports*, vol. 24, no. 10, pp. 2746–2756.e5,
820 Sep. 2018, doi: 10.1016/j.celrep.2018.08.006.
821 [61] M. C. Rajagopal *et al.*, “Materials-to-device design of hybrid metal-polymer heat exchanger
822 tubes for low temperature waste heat recovery,” *International Journal of Heat and Mass
823 Transfer*, vol. 143, p. 118497, Nov. 2019, doi: 10.1016/j.ijheatmasstransfer.2019.118497.
824 [62] M. D. Johnson, J. Völker, H. V. Moeller, E. Laws, K. J. Breslauer, and P. G. Falkowski,
825 “Universal constant for heat production in protists,” *PNAS*, vol. 106, no. 16, pp. 6696–
826 6699, Apr. 2009, doi: 10.1073/pnas.0902005106.

827 [63] R. P. Chhabra, *CRC Handbook of Thermal Engineering*. CRC Press, 2017.

828 [64] M. K. Sato *et al.*, “Temperature Changes in Brown Adipocytes Detected with a Bimaterial
829 Microcantilever,” *Biophysical Journal*, vol. 106, no. 11, pp. 2458–2464, Jun. 2014, doi:
830 10.1016/j.bpj.2014.04.044.

831 [65] G. Kucsko *et al.*, “Nanometre-scale thermometry in a living cell,” *Nature*, vol. 500, no.
832 7460, Art. no. 7460, Aug. 2013, doi: 10.1038/nature12373.

833 [66] G. Baffou *et al.*, “Photoinduced Heating of Nanoparticle Arrays,” *ACS Nano*, vol. 7, no. 8,
834 pp. 6478–6488, Aug. 2013, doi: 10.1021/nn401924n.

835 [67] P. Lee, K. K. Y. Ho, P. Lee, J. R. Greenfield, K. K. Y. Ho, and J. R. Greenfield, “Hot fat in
836 a cool man: infrared thermography and brown adipose tissue,” *Diabetes, Obesity and
837 Metabolism*, vol. 13, no. 1, pp. 92–93, Jan. 2011, doi: 10.1111/j.1463-1326.2010.01318.x.

838 [68] W. D. van Marken Lichtenbelt *et al.*, “Cold-Activated Brown Adipose Tissue in Healthy
839 Men,” *New England Journal of Medicine*, vol. 360, no. 15, pp. 1500–1508, Apr. 2009, doi:
840 10.1056/NEJMoa0808718.

841 [69] A. D. Pickel and C. Dames, “Size and shape effects on the measured peak temperatures of
842 nanoscale hotspots,” *Journal of Applied Physics*, vol. 128, no. 4, p. 045103, Jul. 2020, doi:
843 10.1063/5.0012167.

844 [70] R. K. Jain, S. A. Shah, and P. L. Finney, “Continuous Noninvasive Monitoring of pH and
845 Temperature in Rat Walker 256 Carcinoma During Normoglycemia and Hyperglycemia,” *J
846 Natl Cancer Inst*, vol. 73, no. 2, pp. 429–436, Aug. 1984, doi: 10.1093/jnci/73.2.429.

847 [71] P. M. Gullino, P.-N. Yi, and F. H. Grantham, “Relationship Between Temperature and
848 Blood Supply or Consumption of Oxygen and Glucose by Rat Mammary Carcinomas,” *J
849 Natl Cancer Inst*, vol. 60, no. 4, pp. 835–847, Apr. 1978, doi: 10.1093/jnci/60.4.835.

850 [72] J. Choi *et al.*, “Probing and manipulating embryogenesis via nanoscale thermometry and
851 temperature control,” *PNAS*, vol. 117, no. 26, pp. 14636–14641, Jun. 2020, doi:
852 10.1073/pnas.1922730117.

853 [73] M. Mohammed, Y. Ootsuka, M. Yanagisawa, and W. Blessing, “Reduced brown adipose
854 tissue thermogenesis during environmental interactions in transgenic rats with ataxin-3-
855 mediated ablation of hypothalamic orexin neurons,” *American Journal of Physiology-
856 Regulatory, Integrative and Comparative Physiology*, vol. 307, no. 8, pp. R978–R989, Aug.
857 2014, doi: 10.1152/ajpregu.00260.2014.

858 [74] S. Youssefian, N. Rahbar, C. R. Lambert, and S. Van Dessel, “Variation of thermal
859 conductivity of DPPC lipid bilayer membranes around the phase transition temperature,”
860 *Journal of The Royal Society Interface*, vol. 14, no. 130, p. 20170127, May 2017, doi:
861 10.1098/rsif.2017.0127.

862 [75] J. A. Kenar, “The use of lipids as phase change materials for thermal energy storage,” *Lipid
863 Technology*, vol. 26, no. 7, pp. 154–156, 2014, doi: 10.1002/lite.201400037.

864 [76] A. R. N. Bastos *et al.*, “Thermal properties of lipid bilayers derived from the transient
865 heating regime of upconverting nanoparticles,” *Nanoscale*, vol. 12, no. 47, pp. 24169–
866 24176, 2020, doi: 10.1039/D0NR06989B.

867 [77] T. A. Balasubramaniam and H. F. Bowman, “Temperature Field Due to a Time
868 Dependent Heat Source of Spherical Geometry in an Infinite Medium,” *J. Heat Transfer*, vol. 96,
869 no. 3, pp. 296–299, Aug. 1974, doi: 10.1115/1.3450195.

870 [78] R. T. ElAfandy *et al.*, “Nanomembrane-Based, Thermal-Transport Biosensor for Living
871 Cells,” *Small*, vol. 13, no. 7, Art. no. 7, 2017, doi: 10.1002/smll.201603080.

872 [79] M. H. Sharqawy, J. H. L. V, and S. M. Zubair, “Thermophysical properties of seawater: a
873 review of existing correlations and data,” *Desalination and Water Treatment*, vol. 16, no. 1–3,
874 pp. 354–380, Apr. 2010, doi: 10.5004/dwt.2010.1079.

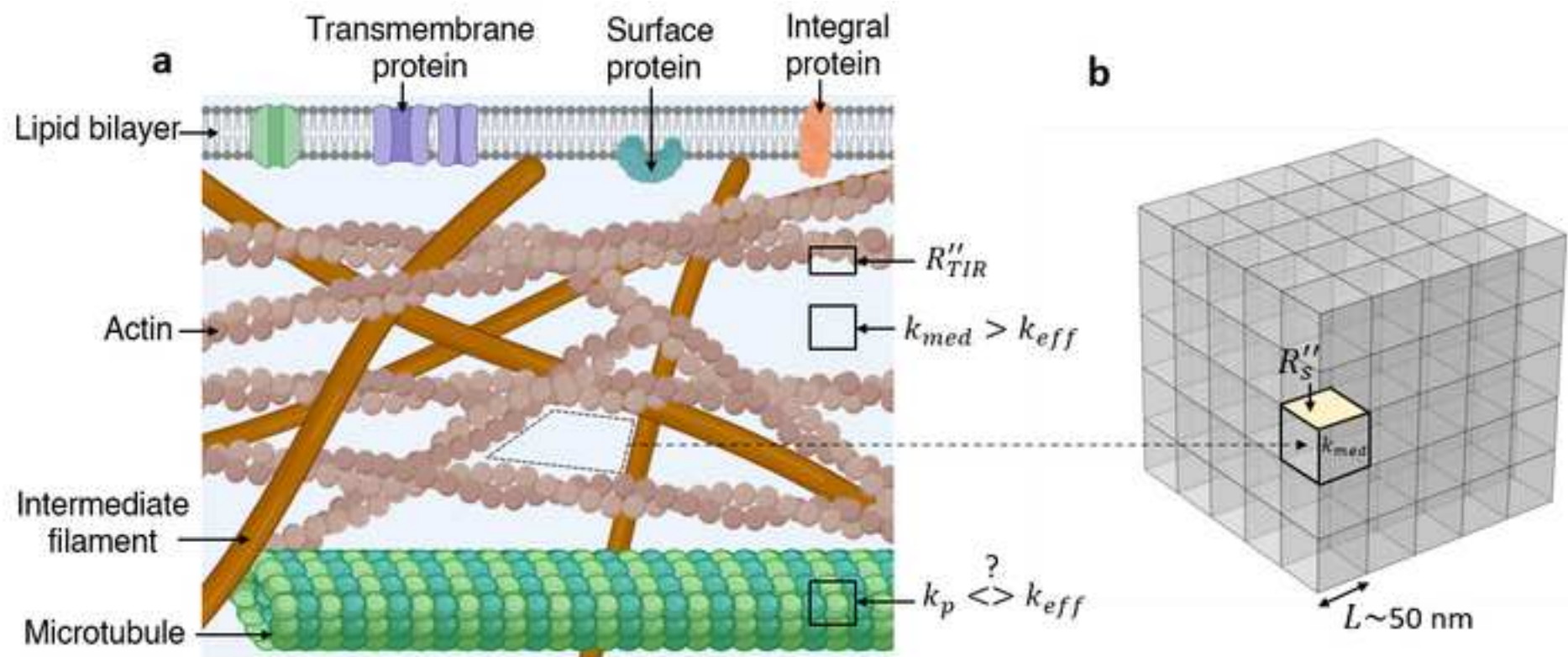
875 [80] K. Arunachalam, P. F. Maccarini, O. I. Craciunescu, J. L. Schlorff, and P. R. Stauffer,
876 “Thermal characteristics of thermobrachytherapy surface applicators for treating chest wall
877 recurrence,” *Phys. Med. Biol.*, vol. 55, no. 7, pp. 1949–1969, Mar. 2010, doi: 10.1088/0031-
878 9155/55/7/011.

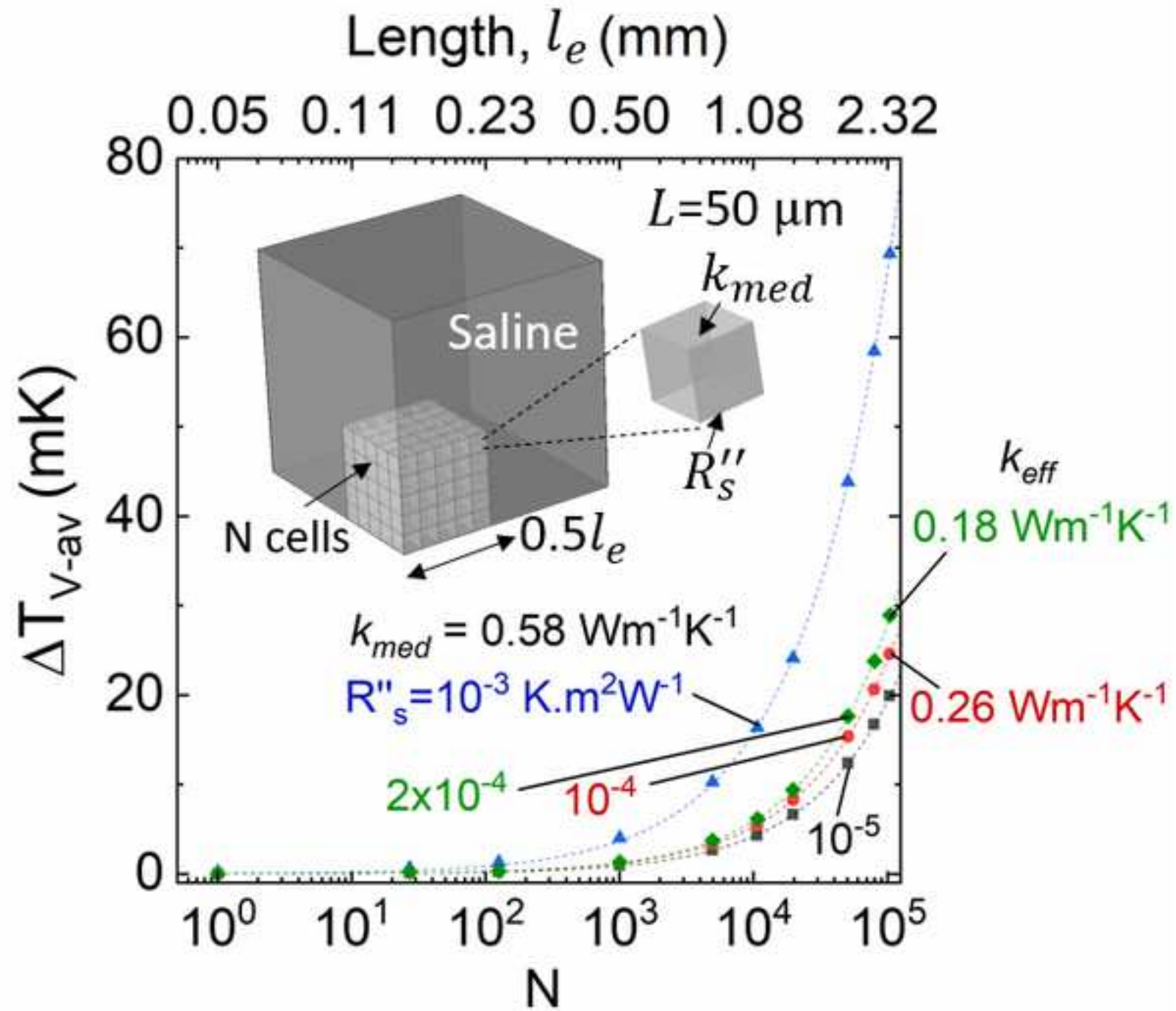
879 [81] K. A. Virtanen *et al.*, “Functional Brown Adipose Tissue in Healthy Adults,”
880 <http://dx.doi.org/10.1056/NEJMoa0808949>, Dec. 2009, doi: 10.1056/NEJMoa0808949.

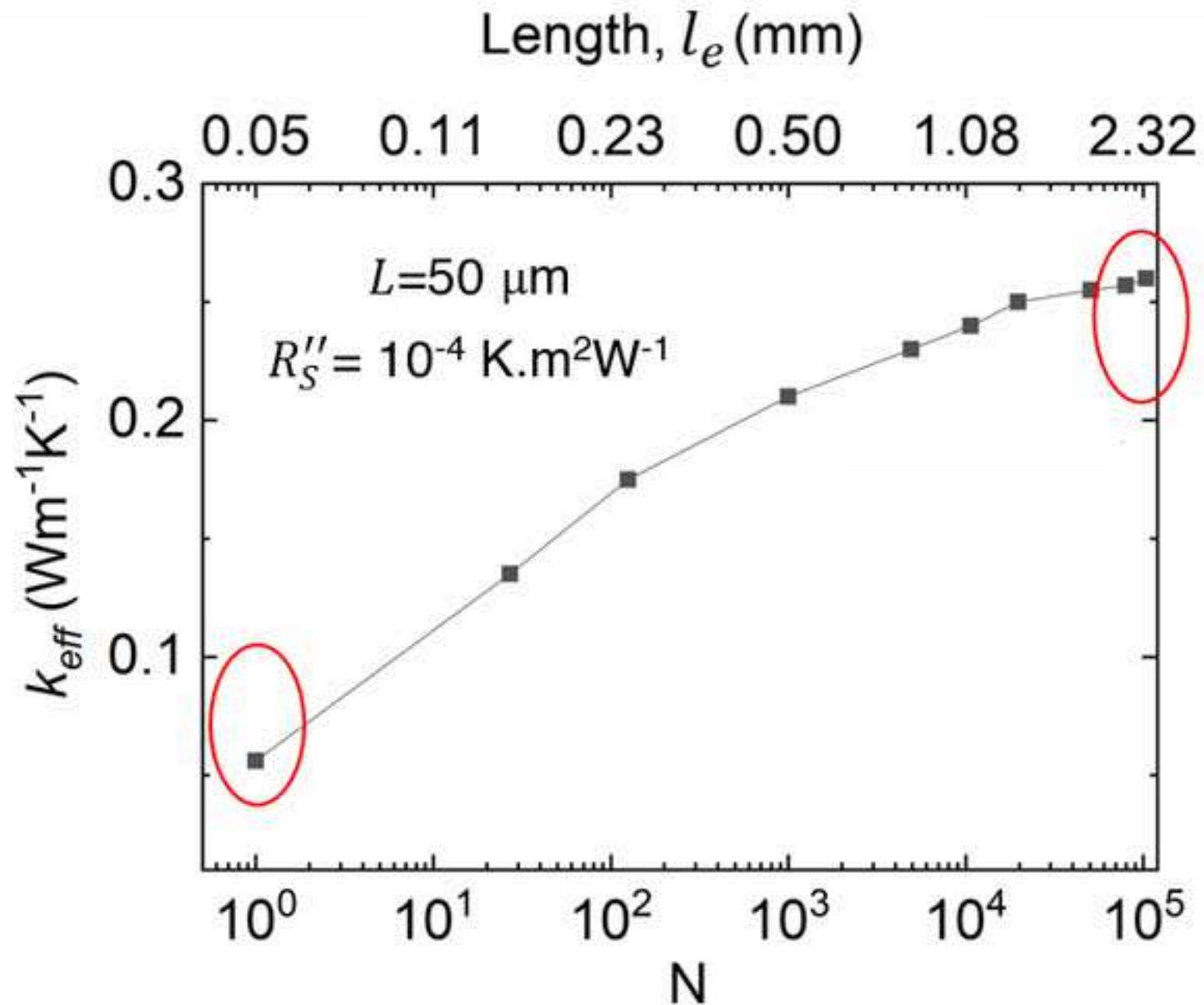
881 [82] A. M. Cypess *et al.*, “Identification and Importance of Brown Adipose Tissue in Adult
882 Humans,” <http://dx.doi.org/10.1056/NEJMoa0810780>, Dec. 2009, doi:
883 10.1056/NEJMoa0810780.

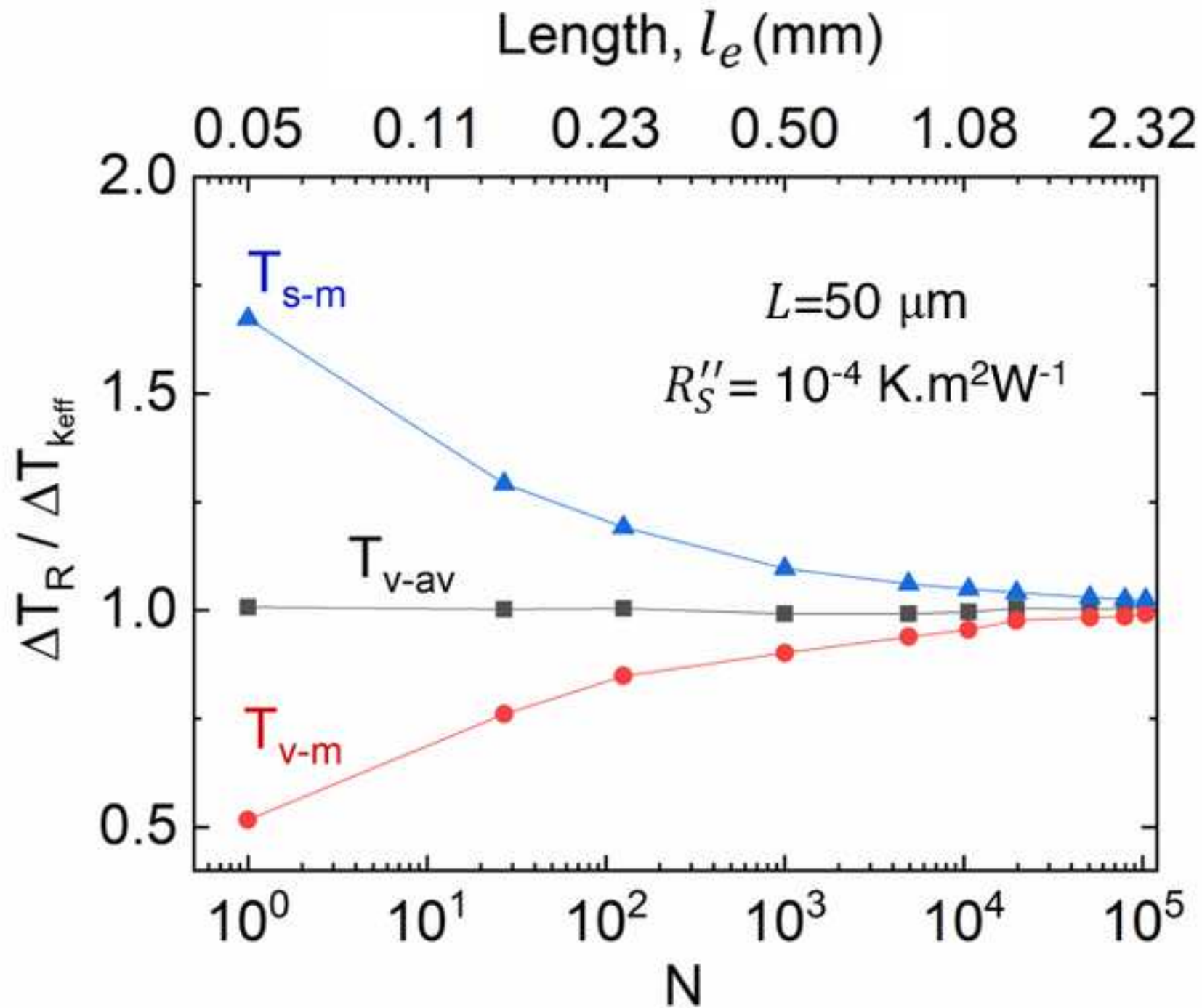
884 [83] V. Vuksanović, L. W. Sheppard, and A. Stefanovska, “Nonlinear Relationship between
885 Level of Blood Flow and Skin Temperature for Different Dynamics of Temperature Change,”
886 *Biophysical Journal*, vol. 94, no. 10, pp. L78–L80, May 2008, doi:
887 10.1529/biophysj.107.127860.

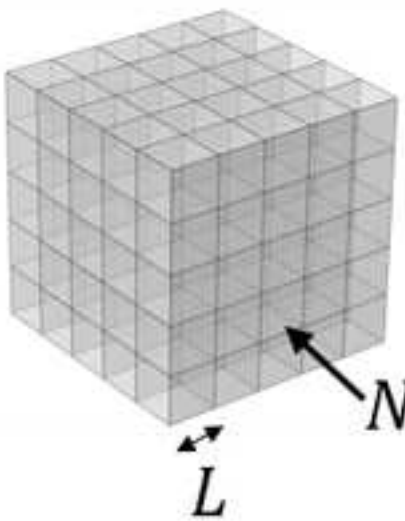
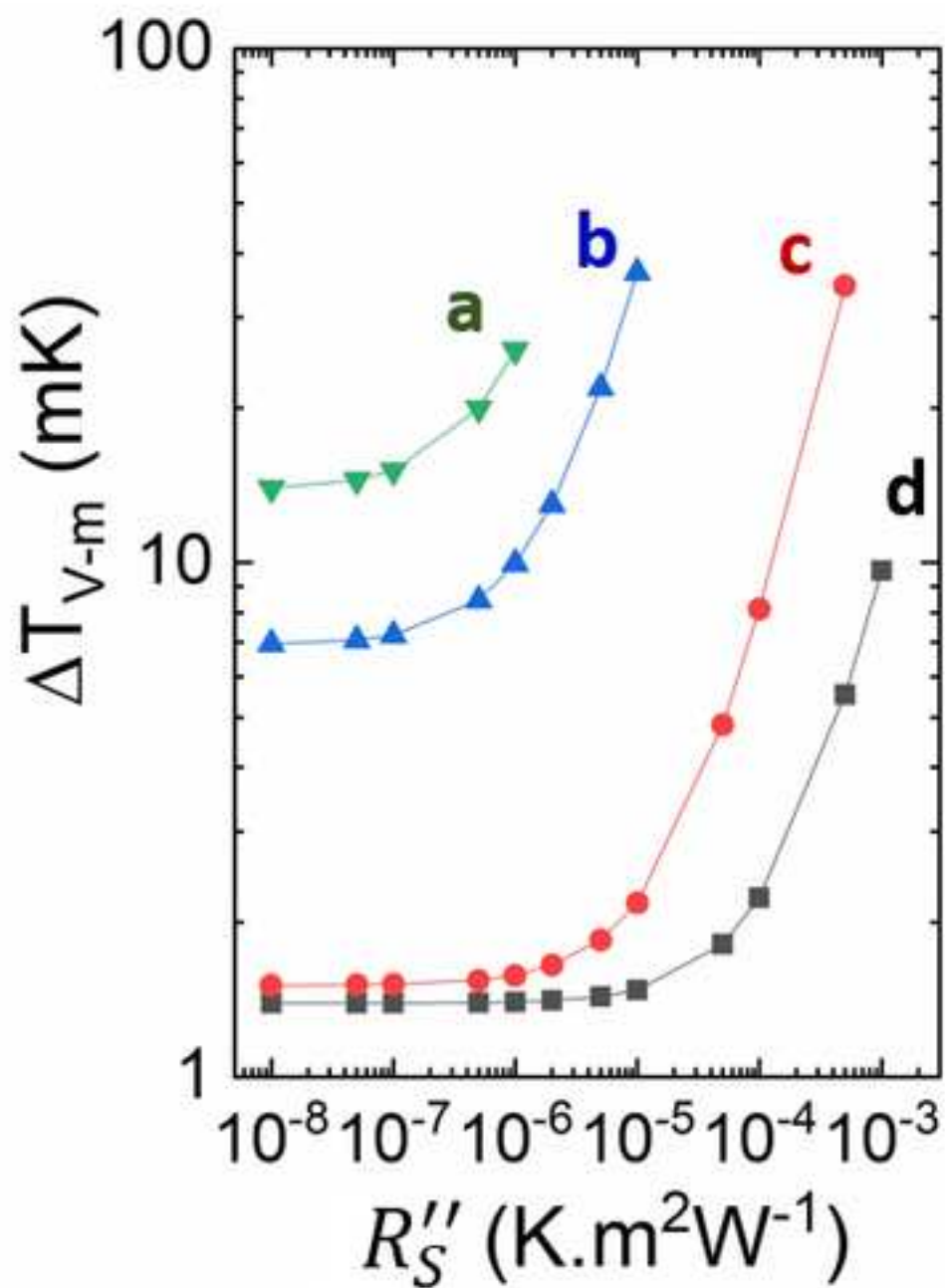
888



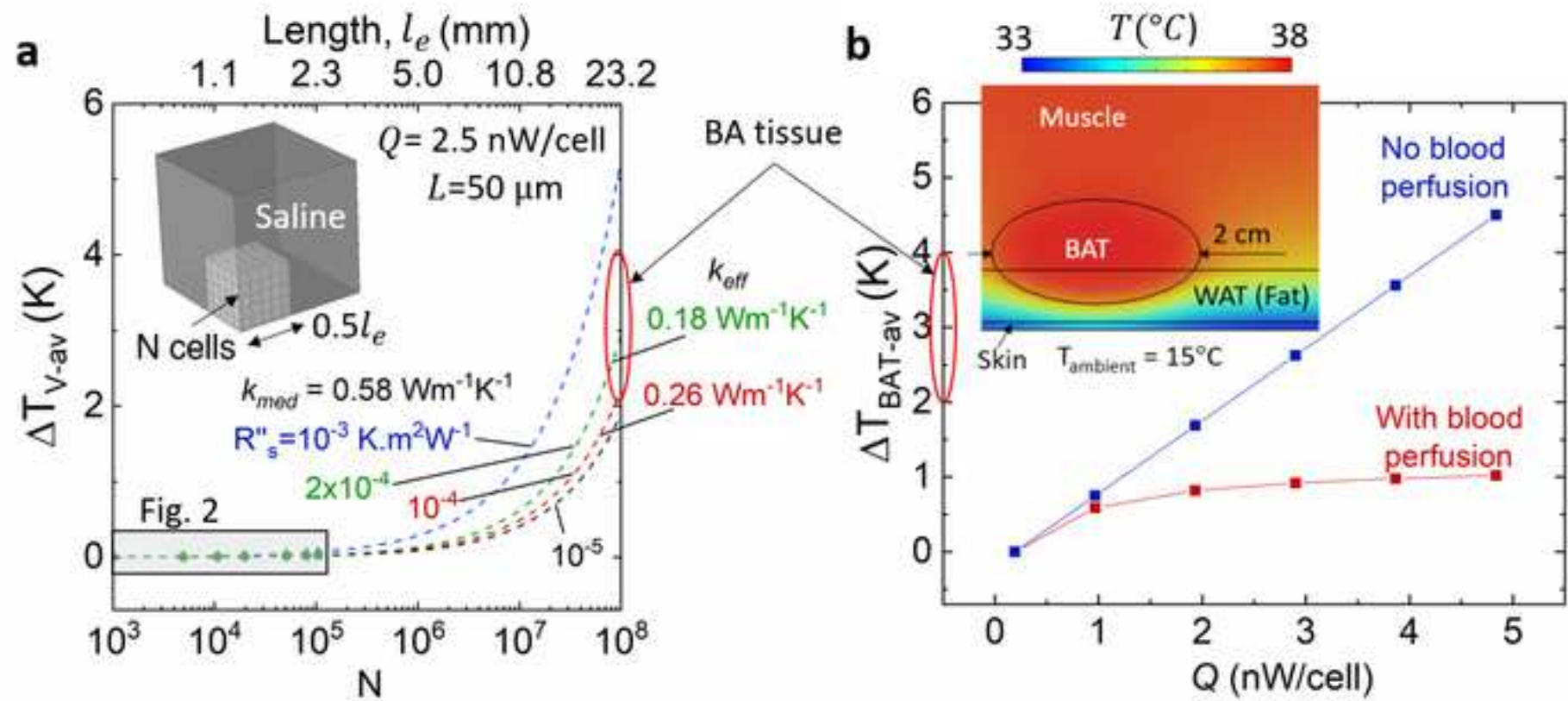








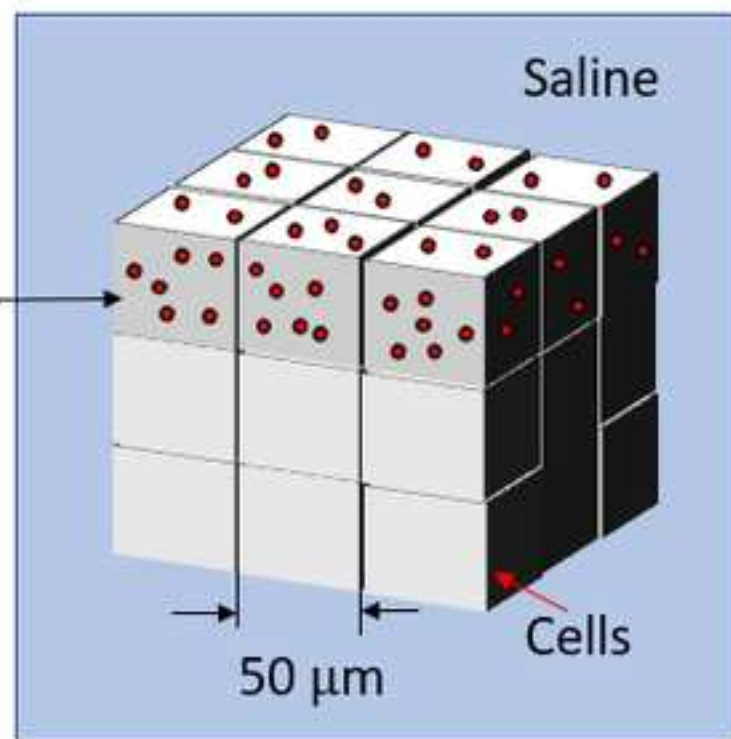
- a:** $N=10000, L=50$ nm, $Q=1$ pW
- b:** $N=10000, L=100$ nm, $Q=1$ pW
- c:** $N=1000, L=1$ μ m, $Q=10$ pW
- d:** $N=10, L=10$ μ m, $Q=1$ nW



a

Intracellular probes
(say, nanoparticles
or molecular)

ΔT_{int}
(maximum ΔT)

**b**

Extracellular probe
(say, RTD or
thermocouple)

ΔT_{ext}
(average ΔT)

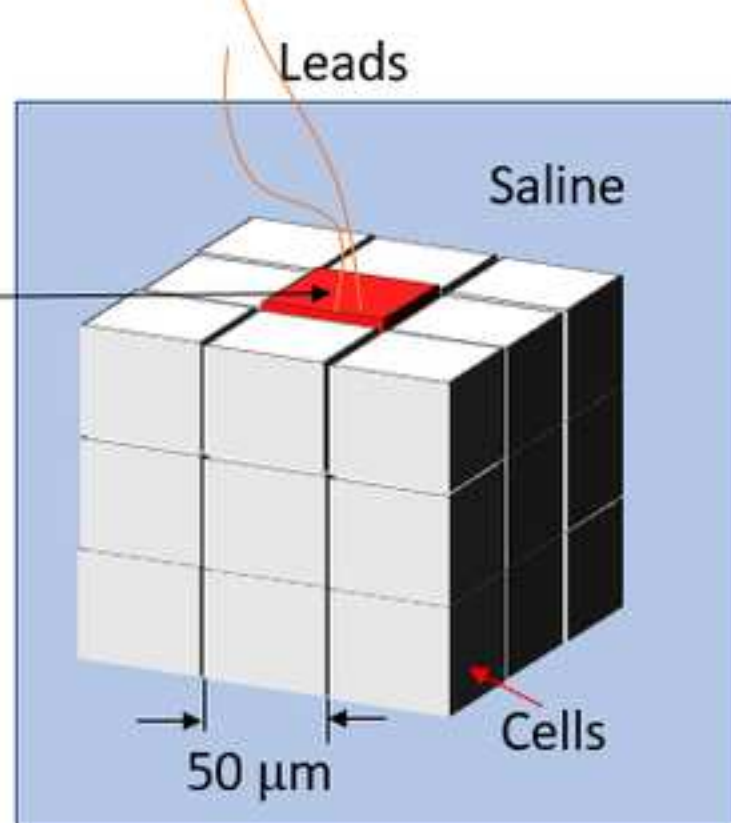
50×50×50 μm^3

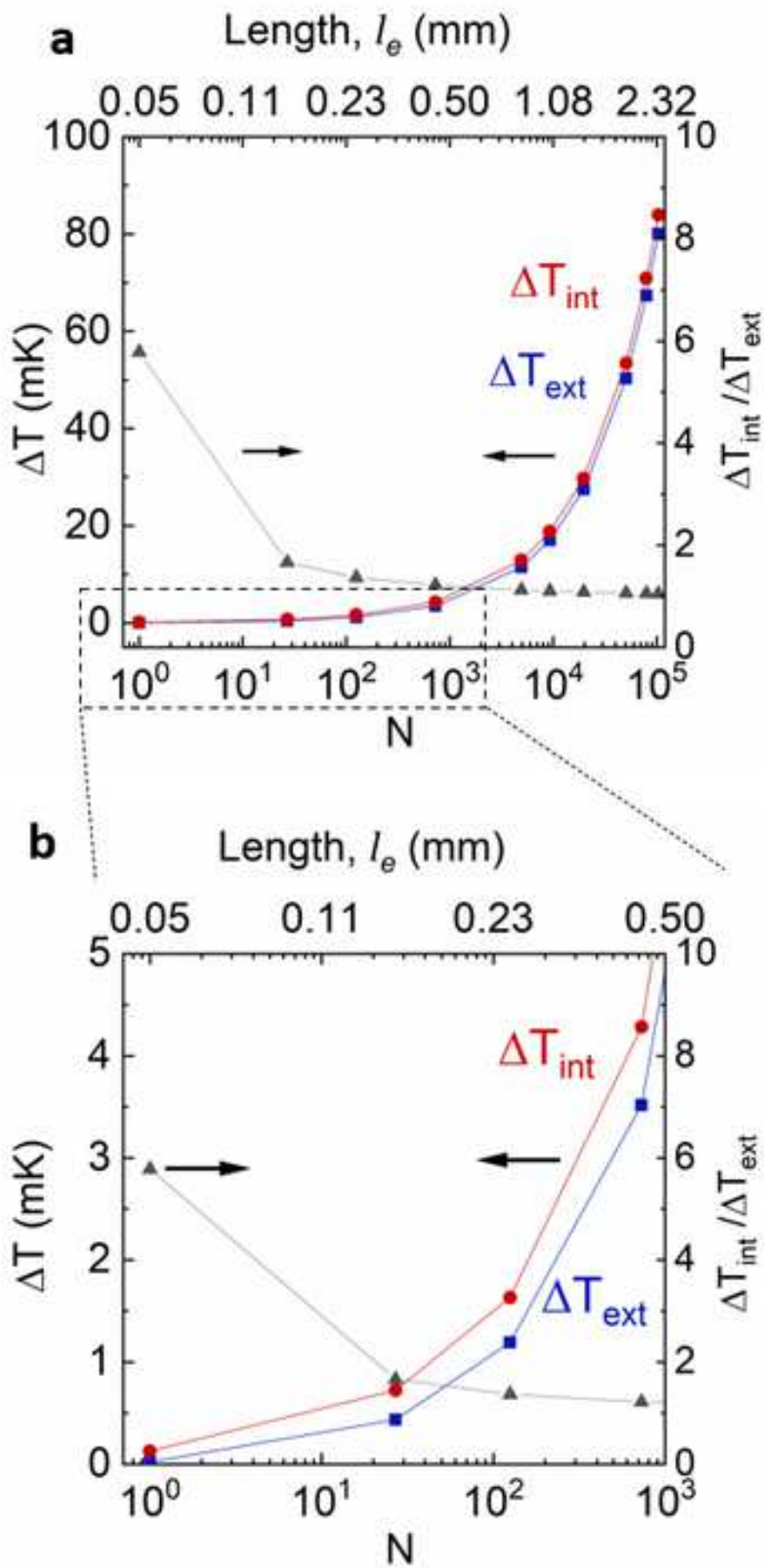
Leads

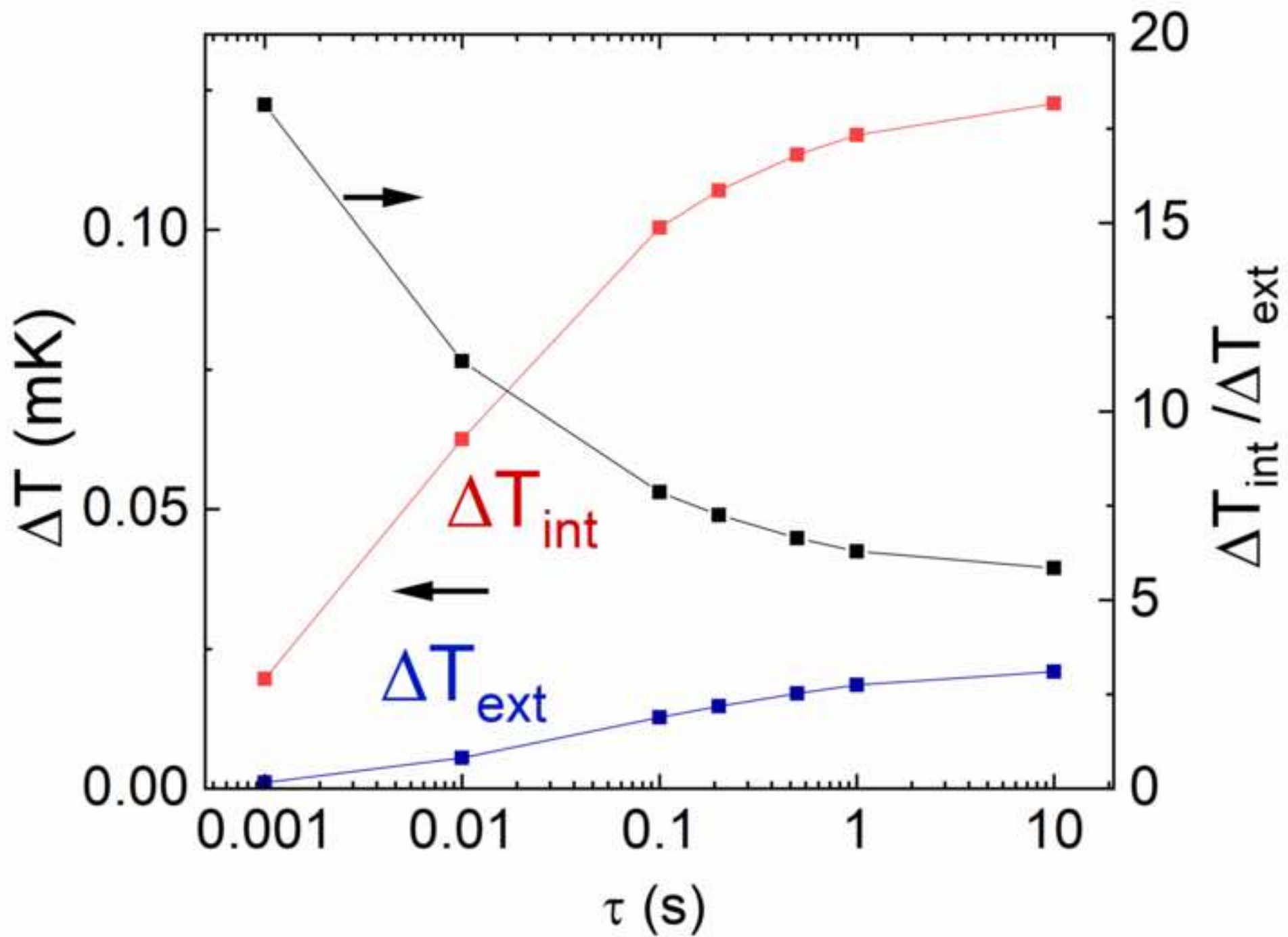
Saline

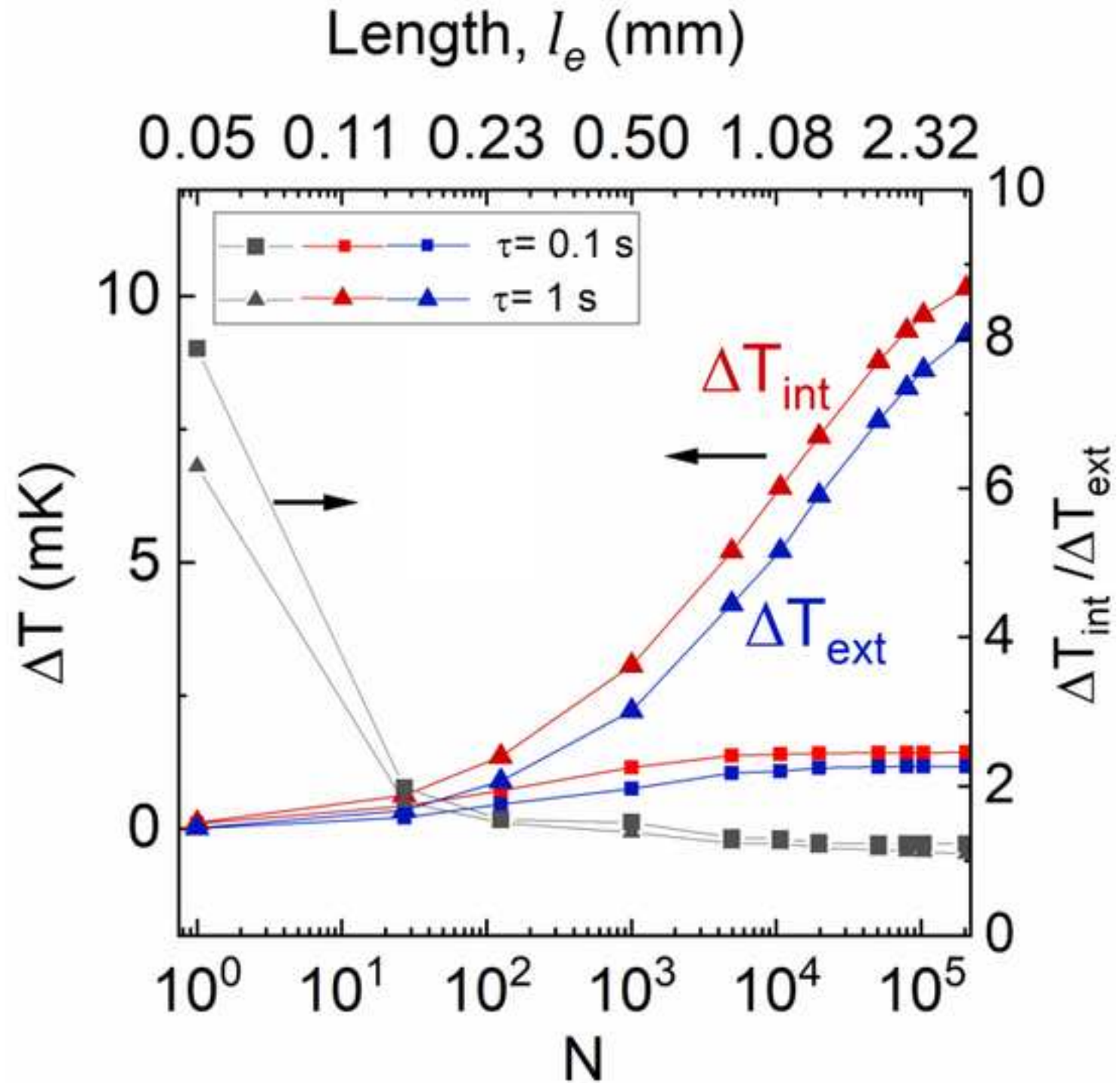
Cells

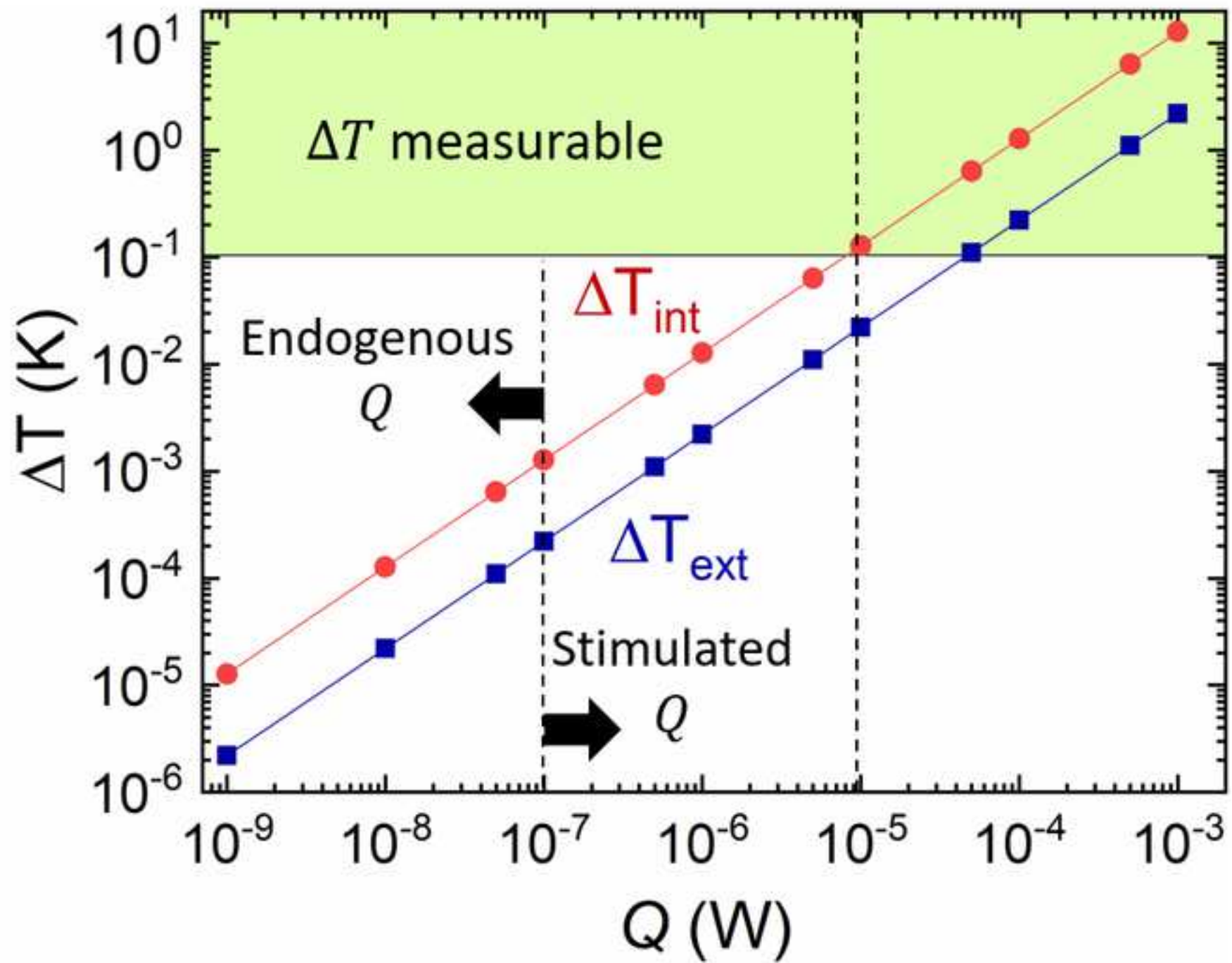
50 μm













Click here to access/download
Supplemental Information
SupplementaryMaterial.pdf